(2)

PENNSTATE

Inhibiting Corrosion in Gr/Al and Gr/Mg Metal Matrix Composites Using Nonequilibrium Alloying Techniques

Annual Report
June 1993

Submitted to
Office of Naval Research
800 North Quincy Street
Arlington, VA 22217-5000

Submitted by:

B.A. Shaw[1], W.C. Moshier[2], R.G. Wendt[2], P.L. Miller[1], T.R. Schrecengost[1], A.E. Krebs[1], and D.J. Ciscon[1]

[1]Penn State University, University Park, PA 16802

[2]Martin Marietta Space Systems, Denver CO 80201

SECURITY CLASSIFICATION OF THIS PAGE

REPORT DOCUMENTATION PAGE

Form Approved OMB No. 0704-0188

1a REPORT SECURITY CLASSIFICATION: Unclassified	1b RESTRICTIVE MARKINGS: None
2a SECURITY CLASSIFICATION AUTHORITY	3. DISTRIBUTION/AVAILABILITY OF REPORT: Unrestricted
2b DECLASSIFICATION/DOWNGRADING SCHEDULE	
4 PERFORMING ORGANIZATION REPORT NUMBER(S)	5. MONITORING ORGANIZATION REPORT NUMBER(S)
6a NAME OF PERFORMING ORGANIZATION: Penn State University; 6b OFFICE SYMBOL (If applicable): Code 1131M	7a. NAME OF MONITORING ORGANIZATION
6c ADDRESS (City, State, and ZIP Code): Dept. of Engineering Science and Mechanics, 227 Hammond Bldg., University Park, PA 16802	7b. ADDRESS (City, State, and ZIP Code)
8a NAME OF FUNDING/SPONSORING ORGANIZATION: Office of Navel Research; 8b OFFICE SYMBOL (If applicable): Code	9. PROCUREMENT INSTRUMENT IDENTIFICATION NUMBER
8c ADDRESS (City, State, and ZIP Code): 800 North Quincy St., Arlington, VA 22217-5000	10. SOURCE OF FUNDING NUMBERS: PROGRAM ELEMENT NO.; PROJECT NO. N00014-91-J-1196; TASK NO.; WORK UNIT ACCESSION NO.

11. TITLE (Include Security Classification)
Inhibiting Corrosion in Gr/Al and Gr/Mg Metal Matrix Composites Using Nonequilibrium Alloying- Second Annual Report

12 PERSONAL AUTHOR(S)
B. A. Shaw, W. C. Moshier, R. G. Wendt, r.L. Miller, T.R. Schrecengost, D. Cison, A. Krebs

13a TYPE OF REPORT	13b TIME COVERED	14. DATE OF REPORT (Year, Month, Day)	15. PAGE COUNT
Technical	FROM 4/1/92 TO 3/31/93	June 25, 1993	77

16. SUPPLEMENTARY NOTATION

17. COSATI CODES			18. SUBJECT TERMS (Continue on reverse if necessary and identify by block number)
FIELD	GROUP	SUB-GROUP	Metal Matrix Composites, Gr/Al Composites, Gr/Mg Composites, Nonequilibrium alloying

19. ABSTRACT (Continue on reverse if necessary and identify by block number)

Metal matrix composites (MMCs) have been heavily studied over the past thirty years. During that period, many proposals have been made to develop a matrix alloy that was compatible with the reinforcing phase. However, for one reason or another, the technology has continued to focus on conventional alloys and fabrication practices. Although tremendous advances have been made on composite materials, the basic technology remains similar to systems studied twenty years ago. This work represents the first new program where new alloys are being developed for graphite reinforced composites which are tailored to a novel processing technology for manufacturing corrosion resistant graphite reinforced composites.

20 DISTRIBUTION/AVAILABILITY OF ABSTRACT	21 ABSTRACT SECURITY CLASSIFICATION	
☒ UNCLASSIFIED/UNLIMITED ☐ SAME AS RPT ☐ DTIC USERS		
22a NAME OF RESPONSIBLE INDIVIDUAL: B. A. Shaw	22b TELEPHONE (Include Area Code): (814) 865-7828	22c OFFICE SYMBOL

DD Form 1473, JUN 86 Previous editions are obsolete SECURITY CLASSIFICATION OF THIS PAGE

PENNSTATE

Inhibiting Corrosion in Gr/Al and Gr/Mg Metal Matrix Composites Using Nonequilibrium Alloying Techniques

Annual Report
June 1993

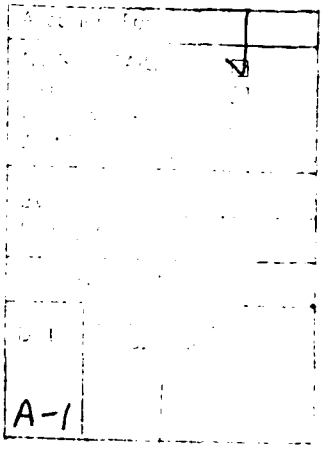

Submitted to
Office of Naval Research
800 North Quincy Street
Arlington, VA 22217-5000

Submitted by:

B.A. Shaw[1], W.C. Moshier[2], R.G. Wendt[2], P.L. Miller[1], T.R. Schrecengost[1], A.E. Krebs[1], and D.J. Ciscon[1]

[1]Penn State University, University Park, PA 16802

[2]Martin Marietta Space Systems, Denver CO 80201

Table of Contents

Introduction

High modulus graphite (Gr) reinforced metal matrix composites (MMCs) offer a wide variety of attractive properties including: high specific modulus and strength (E/ρ and UTS/ρ), tailorable or zero coefficient of thermal expansion (CTE), and high thermal conductivity. Using either Al or Mg as the matrix metal results in a reduction of the final density of the composite with high elastic modulus and excellent strength in the fiber direction. Unfortunately, MMCs, especially Gr reinforced composites, are extremely susceptible to corrosion with severe attack in chloride-containing environments occurring in as little time as several weeks for the Gr/Al composites or in just a few days for Gr/Mg composites.[1]

The overall objective of this research program is to determine whether improving the inherent passivity of the matrix metal in a Gr/Al or Gr/Mg composite can alleviate, or at least minimize, galvanic corrosion between the graphite and the matrix metal. This galvanic corrosion is currently the limiting factor in utilization of these composites. The program focuses on the unique properties of sputter deposited alloys. With sputter deposition it is possibly to significantly increase the solubility of passivity enhancing species in both Al and Mg, thus dramatically improving their corrosion resistance. The approach that is being undertaken is to develop alloy systems capable of minimizing galvanic degradation of the composite. An essential step in this process is identification of alloy compositions which maintain enhanced passivity after processing into the bulk composite. Once these compositions have been identified, then sputter coated fibers can be consolidated into a component by hot isostatic pressing. This research will ultimately lead to the fabrication of a prototype filament-wound mirror support for a starring telescope.

This research will address the following specific issues.

1) Can the passivity of Mg be improved through nonequilibrium alloying or through the use of a cerium based inhibitive treatment?

2) Will these passivity enhanced alloys be compatible with graphite?

3) What are the processing conditions that must be used to make a structure with these materials and still retain the enhanced corrosion performance of the alloys?

4) Can a filament-wound composite structure with improved corrosion performance be fabricated with this technology?

Research to-date has focused on issues 1 through 3 and is summarized in the following section. Detailed information regarding this work is presented in papers which have been submitted for publication (Appendices 1-3). Issue number 4 will be addressed in the final year of the program.

Significant Results from the Past Year

A variety of nonequilibrium Mg alloys have been produced and characterized in this program. Figure 1 shows the anodic polarization behavior for several of these alloys. The most promising corrosion performance has been noted with the addition of Y to Mg. Passivity for these alloys extends several hundred millivolts above E_{oc} and, depending on pH and composition, current densities of a few $\mu a/cm^2$ can be achieved. The significance of the enhanced polarization behavior of these alloys is illustrated in Figure 2. This figure shows galvanic diagrams[2] for Mg-Gr and MgY-Gr couples assuming equal cathode and anode areas. The cross-over point for the anodic and cathodic curves, I_{galv}, is reduced by almost 3 orders of magnitude for the MgY-Gr couple in comparison to I_{galv} for the Mg-Gr couple. Details of this research are presented in Appendix 1.

A separate, but related, investigation is also being conducted to look at the affect of stand-alone inhibitive treatments on the corrosion resistance of Mg. In these experiments, cerium and molybdate treatments are being used to form a protective barrier on Mg surfaces. Initial experiments in this series were based on the work of Mansfeld et al.[3] who identified a $Ce(NO_3)_3/CeCl_3/NaMoO_4$ treatment scheme for significantly improving the corrosion resistance of Al alloys and composites. Our work is still ongoing in this area, but we have found that immersion in hot cerium solutions followed by polarization in sodium molybdate does raise the open circuit potential of Mg and alter its polarization characteristics. Figure 3 shows anodic polarization curves for pure Mg, Mg which has been exposed to $Ce(NO_3)_3$ followed by polarization in $NaMoO_4$, and Mg which has been exposed to both $Ce(NO_3)_3$ and $CeCl_3$ followed by polarization in $NaMoO_4$. The significance of these changes in the polarization behavior on the galvanic compatibility of Mg is illustrated in Figure 4. Galvanic coupling of the treated Mg to an equal area of graphite reduces the galvanic corrosion rate by a factor of approximately 2.7 when compared to untreated Mg.

Work in the past year has focused on further characterization of the nonequilibrium Al alloys and an assessment of the processing conditions needed to maintain enhanced passivity in a consolidated composite. Electrochemical testing of Al-W, Al-Mo, Al-Ta, Al-Ti, and Al-Mg-Ti alloys has revealed that enhanced passivity for these alloys occurs over a wide range of pH. Results for Al-Mo and Al-Mg-Ti alloys are given in Figures 5 and 6, respectively. The fact that passivity occurs over a wide range of pH, where it has been found that the passive film chemistry can change dramatically, has led us to propose a mechanism for the enhanced passivity of these alloys based on a solute-rich interphase between the alloy and the passive film. Details of the mechanism were presented in a paper published in the Journal of the Electrochemical Society in April 1993[4] and in another paper submitted for publication to the same journal in April of this year.[5]

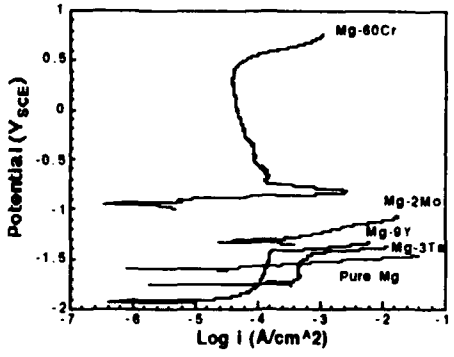

Figure 1. Anodic potentiodynamic polarization curves for different Mg alloys generated in 0.1 M NaCl, pH 8, ambient lab temperature.

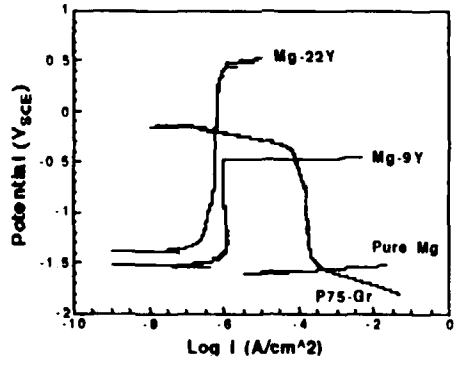

Figure 2. Galvanic diagram for Mg and MgY alloys individually coupled to P75-Gr, all having equal areas of 1.0 cm^2. Curves were generated at a scan rate of 0.05 mV/s in 0.1 M NaCl, pH 12, ambient lab temperature.

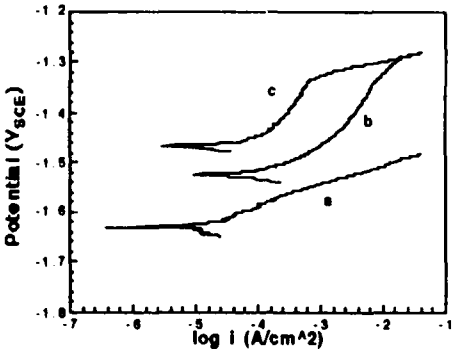

Figure 3. Anodic polarization behavior in 0.1M NaCl at pH 8 for a) untreated Mg, b) treatment 1 - Mg exposed to hot $Ce(NO_3)_3$ for 2 hours followed by exposure to hot $CeCl_3$ for 2 hours followed by polarization in Na_2MoO_4 for 2 hours, c) Mg exposed to hot $Ce(NO_3)_3$ for 4 hours followed by polarization in Na_2MoO_4 for 2 hours.

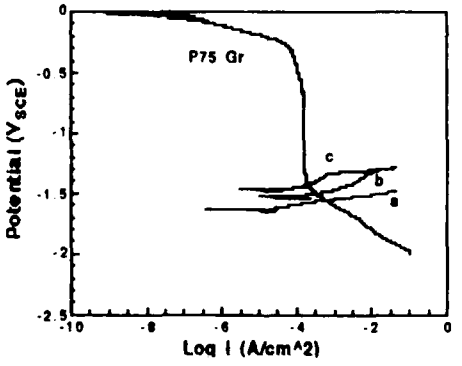

Figure 4. Galvanic diagram for the polarization curves from Figure 3 coupled to P75 graphite with equal cathode and anode areas.

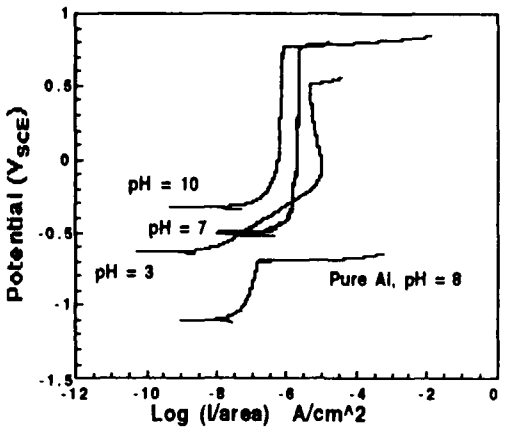

Figure 5. Anodic potentiodynamic polarization plots for Al-19Mo generated at a scan rate of 0.2 mV/s in 0.1 M NaCl at various pHs.

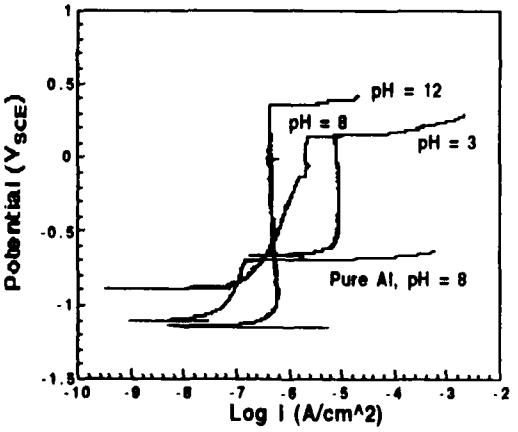

Figure 6. Anodic potentiodynamic polarization plots for Al-5Mg-22Ti generated at a scan rate of 0.2 mV/s in 0.1 M NaCl at various pHs.

Long-term potentiostatic testing (2 week holds on 5 specimens at 5 different potentials) confirmed that passivity was maintained at potentials up to 0.015 V for an Al-26 at.% W alloy. Long-term performance has also been evaluated by monitoring the current as a function of time for the alloys coupled to graphite. Several of the Al-Mo alloys and the Al-26 at.% W alloy, both as-sputtered and heat treated, have been evaluated in these tests. Figure 7 shows the data obtained for pure Al, an Al-19 at.% Mo alloy and an Al-26 at.% W alloy each coupled individually to graphite. Both as-sputtered and heat treated alloys exhibited very low coupled currents and no degradation of the alloys was noted after seven days of coupling. Appendix 2 details the results of these experiments.

For composite applications it is essential that the matrix alloy exhibits the lowest possible density (lower than that of Ti) and that it maintains enhanced passivity at consolidation temperatures (400 to 500°C). Based on these criteria, the Al-Mo system was chosen for further thermal studies. A summary of the results of heat treatments conducted at temperatures of 400, 500, and 600°C are presented in Table 1. At the high solute concentration precipitation of a second phase was observed, only after holding the specimens at 600°C for 8 hours. Stability up to this point has been attributed to the amorphous nature of the high solute concentration alloys. For precipitation of a second phase to occur, the alloy must first crystallize which requires a significant amount of time at a given temperature for these solute concentrations. Thermal stability is also maintained for the 18 at.% Mo alloys at 400°C , but not at 500°C. The 11 at.% Mo alloy precipitated a second phase under all conditions. A detailed account of this investigation is contained in Appendix 3.

To further assess the processing conditions for an Al-Mo based composite, a hot isostatic pressing (HIP) consolidation study was conducted this past year. Initially, an Al-18 at.% Mo alloy was evaluated to establish the parameters required for consolidation. This alloy was selected because it exhibited the low galvanic currents when coupled to graphite and was the lowest density alloy that maintained good corrosion resistance after heat treating at the nominal composite consolidation temperatures. Unfortunately, the Al-18 at.% Mo alloy did not consolidate during these initial trials. Failure to consolidate was attributed to the sluggish kinetics of the alloys (as evident from the lack of precipitation after heat treatment at 400°C) limiting interdiffusion and subsequent bonding. As a result of these findings, further experiments were conducted on a lower solute concentration alloy (Al-11 at.%Mo) and an Al-18 at.%Mo alloy which had an Al-rich surface layer approximately 1000 Å thick. Successful consolidation was achieved for both of these alloys when HIP'ed at a temperature of 500°C and a pressure of 69 MPa for 4 hours. A SEM micrograph revealing consolidation for the Al-18 at.% Mo alloy with an Al interlayer is presented in Figure 8. Based on these results, an Al-Mo alloy with a solute concentration between 11 and 18 at.% Mo will be used in the prototype mirror support structure to be fabricated in the final year of the program.

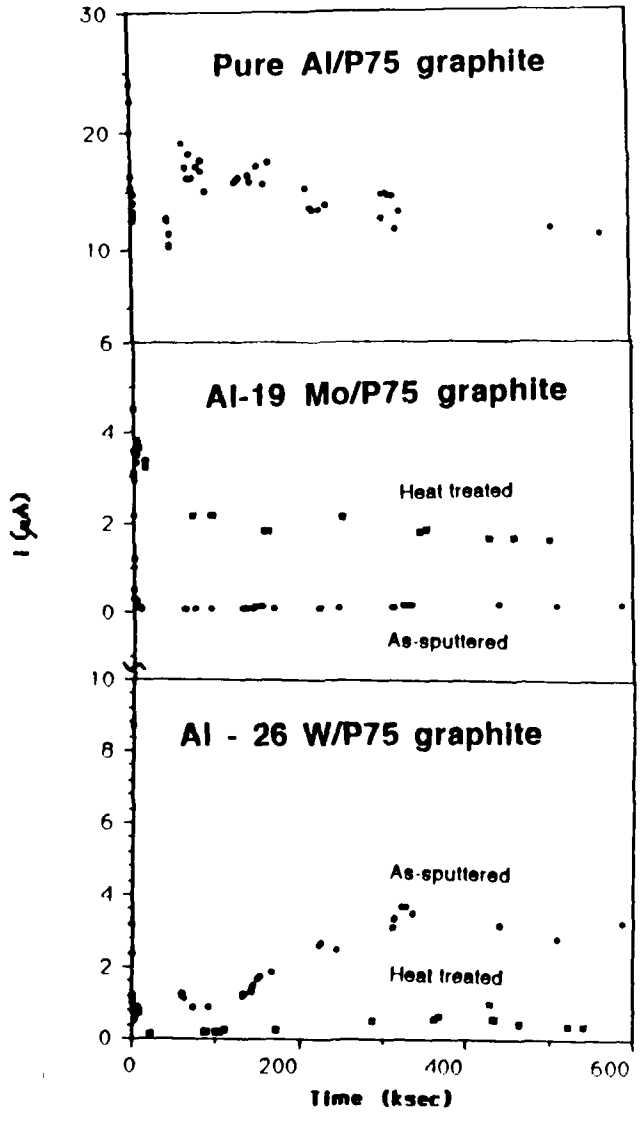

Figure 7 Galvanic current vs time for the as-sputtered pure Al/Gr, and the as-sputtered and heat treated Al-19.1 Mo/Gr and Al-25 9 W/Gr couples in 0.1M NaCl at pH 8 for 7 days (cathode to anode area ratios are 0.11, 0.41, 0 14, 0 14,and 0.43, respectively)

Table 1. Summary of Al-Mo Alloy Structure Following Heat Treatment

Time	400° C	500° C	600° C
8 hrs	Al-11Mo, ppt Al-18Mo, no ppt Al-23Mo, no ppt	Al-18Mo, ppt Al-23Mo, no ppt	Al-23Mo, ppt
4 hrs	Al-11Mo, ppt Al-18Mo, no ppt Al-23Mo, no ppt	Al-18Mo, ppt Al-23Mo, no ppt	Al-23Mo, no ppt
1 hrs	Al-11Mo, ppt Al-18Mo, no ppt Al-23Mo, no ppt	Al-18Mo, ppt Al-23Mo, no ppt	Al-23Mo, no ppt

Temperature

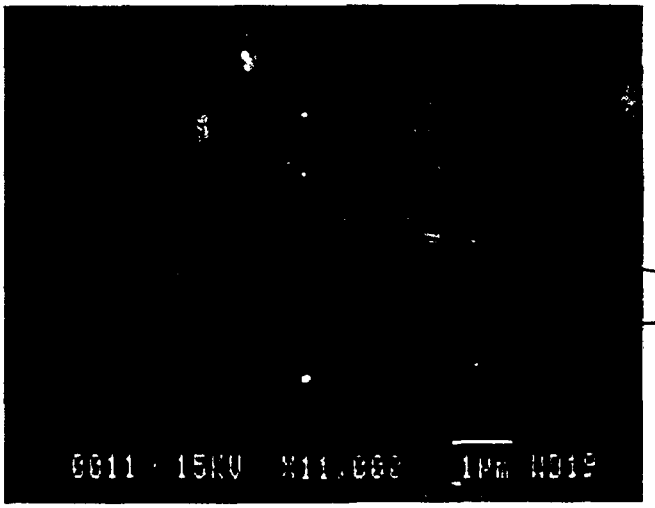

Figure 8. Consolidated Al-18Mo with an Al interlayer. The can material was mild steel and the HIP'ing conditions were 500°C for 4 hrs at 69 MPa.

References

1. P.P. Traskoma, "Corrosion behavior of graphite fiber/magnesium metal matrix composites in aqueous chloride solution," Corrosion, 42, 609 (1986).

2. D.A. Jones, Principles and Prevention of Corrosion, Macmillan Publishing Co., New York, pp. 182-186, (1992).

3. F. Mansfeld, Y. Wang, and H. Shih,"Steps toward a Stainless Al Alloy," NACE Research in Prograss Abstracts, Corrosion 92, Cincinnati, OH.

4. G.D. Davis, B.A. Shaw, B.J. Rees and M. Ferry, "Mechanisms of Passivity of Nonequilibrium Al-W Alloys," J. Electrochemical Society, 140, 951 (1993).

5. G.D. Davis, B.A. Shaw, B.J. Rees, E.L. Principe, and C.A. Pecile, "Electrochemical behavior and surface chemistry of Al-Ta alloys: solute-rich interphase model," submitted to the J. Electrochemical Society April 1993.

Appendix 1

Assessing the Corrosion Resistance of Nonequilibrium MgY Alloys

P.L. Miller, B.A. Shaw, R.G. Wendt, and W.C. Moshier

Assessing the Corrosion Resistance of Nonequilibrium MgY Alloys

P. L. Miller and B. A. Shaw
The Pennsylvania State University, University Park, PA 16802

R. G. Wendt and W. C. Moshier
Martin Marietta Astronautics Group, Denver, CO 80201

Abstract

Magnesium alloyed with yttrium has been made by co-sputter deposition. Anodic potentiodynamic polarization experiments were conducted at various scan rates and pH values to assess the corrosion resistance of several MgY alloys. These alloys exhibited enhanced corrosion behavior when compared to pure Mg. Differences included higher breakdown potentials, lower passive current densities, and increased galvanic compatibility.

Introduction

Magnesium (Mg) alloyed with Yttrium (Y) is currently being investigated for use as the matrix metal in graphite (Gr) reinforced metal matrix composites (MMCs). A Gr/Mg MMC would result in a light-weight composite with high elastic modulus and strength in the fiber direction. However, a major problem associated with Mg is its severe susceptibility to corrosion (both uniform and galvanic), especially in chloride-containing environments.[1-3] The study by Trzaskoma showed that Gr/Mg MMCs immersed in a very dilute chloride solution, 0.001 N NaCl, were severely corroded in only five days.[2] Corrosion was attributed to the rapid reaction of Mg with water and galvanic coupling between the Mg matrix and Gr fibers.

This paper investigates the polarization behavior of nonequilibrium MgY alloys and compares these results to that of pure bulk Mg. Enhanced anodic polarization behavior should improve both the galvanic compatibility between the graphite and MgY alloy and increase the alloy's uniform corrosion resistance.

Experimental

MgY alloys were fabricated using co-sputter deposition. Two targets, pure Mg (99.9 %) and pure Y (99.95 %), were sputtered onto single crystal silicon substrates, yielding a MgY film approximately 2 μm thick. The substrate was rotated at a rate of 30 rpm during deposition to ensure a uniform solute concentration across the film. Two alloys, Mg-9$^{a}/_{o}$Y and Mg-22$^{a}/_{o}$Y, were fabricated for evaluation and testing. Yttrium concentrations were estimated using semi quantitative energy dispersive spectroscopy (EDS).

Samples for corrosion testing were fabricated by cleaving the coated Si wafer into 16 pieces, each with an area of approximately 4 to 5 cm^2. Individual pieces were then coupled to a potentiostat through a lead wire and all regions, except the test area, were coated with an adherent marine epoxy (Interlux 404/414) to insure that environmental and electrical isolation were maintained. Anodic potentiodynamic polarization of all materials was carried out using an EG&G PAR Model 273 Potentiostat interfaced with a personal computer. All testing was conducted at ambient lab temperature (25°C) in quiescent, 0.1 M NaCl solution at pH values of 8, 10, and 12 adjusted using dilute NaOH. A conventional three electrode technique, consisting of a saturated calomel reference electrode (SCE), graphite counter electrodes, and sample electrode, was used to measure polarization behavior. All reported potential values were referenced to a SCE. The anodic scans were generated at both 0.2 and 0.05 mV/s, with a minimum of two anodic polarization curves generated for each condition. Prior to each anodic polarization, the corrosion potential (E_{oc}) was allowed to stabilize for approximately 30 min. The data were corrected for IR drop every 10 seconds using the current interrupt feature of the potentiostat.

Results and Discussion

Figure 1 shows anodic polarization curves for Mg, Mg-9$^a/_o$Y, Mg-22$^a/_o$Y, and Y, generated at a scan rate of 0.2 mV/s in 0.1 M NaCl at a pH of 8. The polarization curves for Mg were generated using bulk Mg, while sputtered films were used for the Y and MgY alloys. E_{oc} values observed for sputtered Mg were similar to those of bulk Mg with sputtered Mg being 120 to 140 mV more electrochemically active than bulk Mg. Sputtered Mg was not used because of its extremely rapid degradation in both the atmosphere and in solution. At a pH of 8, Mg-22$^a/_o$Y maintained a lower passive current density (i_{pass}), whereas the Mg-9$^a/_o$Y alloy displayed the higher breakdown potential (E_b). Values for i_{pass} ranged from 0.7 to 4.9 $\mu A/cm^2$ for Mg-22$^a/_o$Y while values for Mg-9$^a/_o$Y were between 40 and 128 $\mu A/cm^2$. E_b values for Mg-9$^a/_o$Y ranged from -1398 to -1460 mV, whereas those for Mg-22$^a/_o$Y were between -1543 and -1597 mV. E_{oc} for both alloys decreased with the addition of Y to Mg. Lower E_{oc} values for the MgY alloys when compared to pure Mg are probably a result of differences in Tafel behavior and exchange current density (i_o). Mg exhibits an i_o value which is greater than that of Y.[4] Therefore, when alloying Mg with Y, a lower E_{oc} value could be obtained. These trends also apply to anodic polarization curves generated at the scan rate of 0.05 mV/s. The slower scan rate curves were generated to ensure that decreasing the scan rate did not adversely affect E_b. Increasing the solution pH from 8 to 10 yielded little change in the anodic polarization behavior of the MgY alloys. The only notable difference was an increase in E_b (approximately 100 mV) for the Mg-22$^a/_o$Y alloy. When compared to that of pure Mg, anodic polarization curves for MgY alloys generated at pH 8 and 10 exhibited increased corrosion resistance, which should result in better galvanic compatibility when used as the matrix metal in a graphite reinforced MMC.

Changing solution pH from 10 to 12 resulted in significant changes in the polarization behavior of the MgY alloys. Based on thermodynamic behavior

alone,[5] one would expect Mg to have better corrosion resistance at pH values above approximately 11.6. Figure 2 shows anodic polarization curves for pure Mg, Mg-9$^a/_o$Y, Mg-22$^a/_o$Y, and pure Y generated at a scan rate of 0.05 mV/s in 0.1 M NaCl, pH = 12. Values of i_{pass} for the Mg-22$^a/_o$Y alloys were lower (0.5 $\mu A/cm^2$) than those of the Mg-9$^a/_o$Y alloys (1.3 $\mu A/cm^2$). E_{oc} values, when compared to values observed at pH 8 and 10, were more electrochemically noble in the pH 12 solution. Values of E_b for both alloys tested at pH 12 varied from -465 to -972 mV for Mg-9$^a/_o$Y and +340 to -92 mV for the Mg-22$^a/_o$Y alloy. The wide range of E_b values is believed to be due to film defects created during the sputtering and handling processes.[1] In contrast to the anodic polarization curves generated at pH 8, E_b for the alloy containing high concentrations of Y was consistently more noble.

More noble values of E_b and lower i_{pass} values are quite important when looking to couple MgY to a noble material such as graphite. For good galvanic corrosion resistance, the coupled current density (i_{galv}) needs to be within the passive region of the anodic polarization curve so that a small shift in potential will not adversely affect i_{galv}. Lower passive current densities of these alloys also result in decreased values for i_{galv}. Figure 3 shows a galvanic diagram[6] for Mg and MgY alloys individually coupled to P75-Gr, all having equal areas of 1.0 cm^2. These curves were generated at the slower 0.05 mV/s scan rate. The most corrosion resistant alloy exhibited an i_{galv} of 0.7 $\mu A/cm^2$, whereas that of pure Mg was 400 $\mu A/cm^2$. This represents a significant increase in galvanic compatibility for a Mg reinforced composite. To ensure good galvanic compatibility, E_b for the MgY matrix must be greater than E_{oc} for the graphite fibers. Thus far, three anodic potentiodynamic polarization tests (two tested at the scan rate of 0.05 mV/s and one at 0.2 mV/s in pH 12 solution) have exhibited this behavior. Specimens that broke down at potentials below the E_{oc} of graphite may have done so due to defects in the film. Even with the variability in E_b, all the MgY alloys tested showed increased galvanic compatibility when coupled to P75-Gr.

Conclusions

1. Addition of Y to Mg significantly alters its polarization behavior. These differences include increased E_b, lower i_{pass} values, and increased galvanic compatibility when compared to pure Mg.

2. Both MgY alloys exhibited much greater corrosion resistance when tested in 0.1 M NaCl solution at a pH of 12. This is believed to be the best polarization behavior exhibited to date by a Mg alloy. Values for E_b varied at the high pH. This range in E_b is believed to be due to defects incurred during fabrication and handling of the thin film alloy.

3. A significant increase in galvanic compatibility between graphite and Mg is observed when alloying Mg with Y.

Acknowledgment

This research was funded by A. J. Sedriks of the Office of Naval Research under contract number N00014-91-J-1196.

References

1. T. R. Schrecengost, B. A. Shaw, R. G. Wendt, and W. C. Moshier, Nonequilibrium Alloying of Magnesium with Chromium to Enhance Passivity and Limit Corrosion in Graphite/Magnesium Composites, Submitted to Corrosion.

2. P. P. Trzaskoma, Corrosion, **42** (10), 609 (1986).

3. V. Mitrovic-Scepanovic and R. J. Brigham, Corrosion, **48** (9), 780 (1992).

4. J. M. West, Electrodeposition and Corrosion Processes, Van Nostrand Reinhold, London, 50, (1965).

5. M. Pourbaix, Atlas of Electrochemical Equilibria in Aqueous Solutions, Houston, Texas, NACE, 141, (1974).

6. D. A. Jones, Principles and Prevention of Corrosion, 1st ed., Macmillan Publishing Co., New York, NY, 167 - 188, (1992).

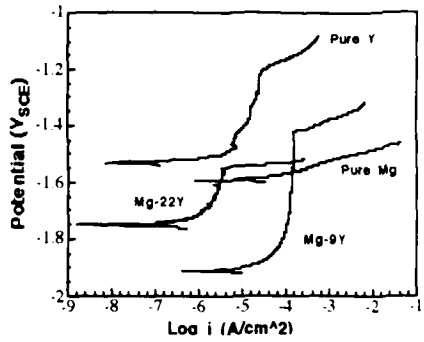

Figure 1. Anodic potentiodynamic polarization curves for Mg, Mg-9$^{a}/_{o}$Y, Mg-22-$^{a}/_{o}$Y, and Y, generated at a scan rate of 0.2 mV/s in 0.1 M NaCl, pH 8, 25° C.

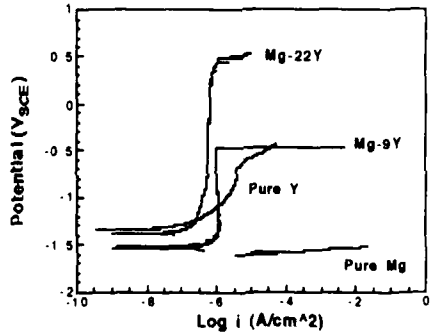

Figure 2. Anodic potentiodynamic polarization curves for Mg, Mg-9$^{a}/_{o}$Y, Mg-22$^{a}/_{o}$Y, and Y generated at a scan rate or 0.05 mV/s in 0.1 M NaCl, pH 12, 25° C.

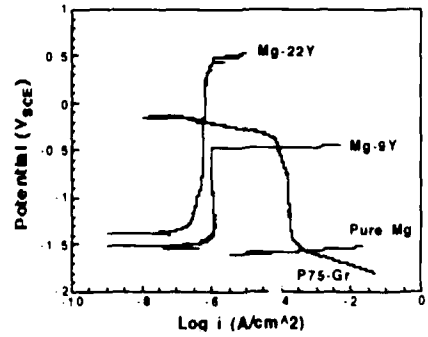

Figure 3. Galvanic Diagram for Mg and MgY alloys individually coupled to P75-Gr, all having equal areas of 1.0 cm^2. Curves were generated at a scan rate of 0.05 mV/s in 0.1 M NaCl, pH 12, 25° C.

Appendix 2

Nonequilibrium Alloying for Improving the Corrosion Resistance of Graphite-Reinforced Aluminum Metal Matrix Composites

T R. Schrecengost, B.A. Shaw, R.G. Wendt, and W.C. Moshier

(Accepted for publication in Corrosion)

Nonequilibrium Alloying for Improving the Corrosion Resistance of Graphite-Reinforced Aluminum Metal Matrix Composites

T.R. Schrecengost and B.A. Shaw
The Pennsylvania State University, University Park, PA 16802

R.G. Wendt and W.C. Moshier
Martin Marietta Astronautics Group, Denver, CO 80201

ABSTRACT

With superior corrosion behavior compared to pure Al, nonequilibrium Al alloys produced by co-sputter deposition have great potential for use as matrix metals in graphite-reinforced aluminum composites. These composites are of current interest because of their enhanced specific properties which result from a low density matrix and a high modulus reinforcing fiber. Co-sputter deposited Al alloys provide a means for improving the inherent corrosion resistance of Al and also removing a conventional processing step that accelerates degradation of the composite once the graphite fibers are exposed.

Additions of W and Mo dramatically enhance the localized corrosion resistance of Al. At concentrations of 19 $^{a}/_{o}$ Mo or 26 $^{a}/_{o}$ W, breakdown potentials are increased by 1115 mV and 1245 mV over pure Al, respectively. Heat treatment of these alloys at 400 °C for 1 hour does not result in precipitation of a second phase and these alloys maintain their excellent resistance to localized attack. Galvanic current diagrams predict that the use of these alloys in composite structures would decrease galvanic corrosion rates by at least two orders of magnitude. This enhancement in galvanic corrosion resistance is a result of the significant improvements in passivity which occur with the nonequilibrium addition of either Mo or W to Al. Galvanic current measurements confirm the predicted reduction in galvanic corrosion rates for these alloys.

INTRODUCTION

Graphite fiber reinforced metal matrix composites (MMCs) are under development for a variety of structural aerospace applications. Using Al as the matrix metal results in a reduction of the final density of the composite with high elastic modulus and excellent strength in the fiber direction. High modulus graphite fiber reinforced composites offer a wide variety of attractive properties including high specific modulus, tailorable or zero coefficient of thermal expansion, and high thermal conductivity. With these properties, structures can be designed and fabricated from MMCs that are dimensionally stable when subjected to both thermal and mechanical loads. Unfortunately, graphite/aluminum (Gr/Al) MMCs are susceptible to severe corrosion, and in marine environments, pitting and extensive galvanic corrosion have been reported for these composites after only a few weeks of exposure.[1-3]

The mechanisms behind the rapid attack of graphite-reinforced composites depend upon the fiber, matrix material, and processing conditions In the literature, pitting,[1,4,5] galvanic corrosion,[3,4,6,7] residual chlorides,[8] and second phase particles[2,5,9] are all reported to contribute to the corrosion of Gr/Al MMCs. It is generally agreed that degradation of Gr/Al MMCs initiates at pits in the Al matrix. Residual chlorides and/or carbides that are produced at the matrix-fiber interface during conventional fabrication accelerate the propagation of attack. Once the graphite fibers are exposed, rapid corrosion of the Al matrix is driven by the cathodic, oxygen reduction reaction on the exposed fibers Final mechanical failure occurs as a result of disbonding or exfoliation of the composite structure.

In order to improve the corrosion resistance of Gr/Al MMCs, researchers have investigated the use of cathodic protection,[8] cathodic inhibitors,[8,9] and barrier coatings.[1,2,4] Cathodic protection can be detrimental because it leads to the formation of hydroxyl ions, and it is not recommended since Al is susceptible to corrosion in alkaline environments. Inhibitors such as $ZnCl_2$ can be used to form $Zn(OH)_2$ precipitates on cathodic sites to reduce the cathodic area and decrease galvanic corrosion. However, this method is not practical for use on composites. Protective coatings such as electroplated[2] or electroless[1,4] Ni, anodization,[1,4] and organic coatings[2] have been used to extend the time for the composite's outer surface to be penetrated by localized corrosion or to seal flaws on the composite's surface. Coatings can easily be damaged and may also be detrimental in space systems because they could interfere with dimensional tolerances, increase composite density, or flake off, which may interfere with sensitive surfaces on space hardware such as detectors and reflectors. Because these methods, for the most part, only delay pitting and galvanic corrosion, they are not permanent solutions to the problem Any permanent solution to the corrosion of graphite-reinforced MMCs needs to improve the inherent corrosion resistance of the matrix metal and remove corrosion accelerating species (residual chlorides and carbides) from the matrix-fiber interface.

In the past, nonequilibrium Al alloys containing several atomic percent W Ta, Cr, or Mo have been shown to significantly improve the localized corrosion resistance of Al, shifting the breakdown potential over 2 V in some cases [10-13] Figure 1 compares the polarization behavior for these alloys to the breakdown potential of pure Al The highest corrosion and breakdown potentials were noted for the high solute concentration Al-Mo and Al-W alloys The mechanism or mechanisms, responsible for the improved passivity of these alloys are still under investigation, but recent results indicate that oxide film structure and a solute-rich metal/passive film interface play key roles Previous results have shown that at low and intermediate solute concentrations precipitation of a second phase occurs with heat treatment at 400 °C for 1 hour and corrosion performance is degraded The use of nonequilibrium alloys as the matrix metal in a graphite-reinforced composite could significantly improve performance as long as the passivity enhancing solute remains in solid solution with the Al during fiber consolidation at elevated temperatures Hot isostatic pressing (HIPing) can be performed as a relatively low temperature consolidation

process; however, it will require temperatures near 400 °C. Therefore, the stability of these alloys at 400°C is critical for the ultimate performance of the composite. Direct sputter deposition of these nonequilibrium alloys onto graphite fibers would also circumvent the problems associated with residual chlorides and carbides at the matrix-graphite interface which occur with conventional processing and contribute to degradation of the composite structure.

Although pitting resistant nonequilibrium alloys can be produced, flaws may still be present in the composite that will allow galvanic corrosion to occur. A variety of researchers have successfully used polarization data to predict galvanic corrosion rates.[8,16-18] Superimposition of anodic and cathodic polarization behavior to form galvanic current diagrams for estimating galvanic corrosion rates was first suggested by Bennett and Greene in 1972.[16] As described in this reference, these diagrams are a convenient tool for estimating corrosion rates for galvanic couples when there is an insignificant IR drop between the two members, the contribution of other anodic and cathodic reactions is very small, and the current density is uniform.[18] Area differences for the coupled metals can be accommodated by simply multiplying the polarization curves by the respective wetted surface areas. These diagrams are useful in helping to assess the galvanic corrosion behavior of couples; however, these predictions should be confirmed with direct galvanic current measurements.

The objectives of this research were to evaluate the effects of heat treatment and galvanic coupling on the corrosion performance of nonequilibrium Al-19 $^{a}/_{o}$ Mo and Al-26 $^{a}/_{o}$ W alloys. Retention of a single phase structure at composite consolidation temperatures and concomitant undiminished corrosion behavior are important to the ultimate performance of the composite. Specimens heat treated at 400 °C for 1 hour were evaluated by X-ray diffraction (XRD) and anodic polarization to see if precipitation and subsequent loss of corrosion resistance occurred. Likewise, galvanic compatibility with graphite is of extreme importance and was evaluated through the use of galvanic current diagrams and galvanic current measurements.

EXPERIMENTAL

Al alloys were produced by RF and DC magnetron co-sputter deposition using a 602RS Thin Film Deposition System. In the co-sputter deposition process, which has been described in detail elsewhere,[19,20] two targets (Al and Mo or Al and W) were used to deposit the alloy onto a polished single crystal silicon wafer (10 cm in diameter). The substrate stage was rotated at a speed of 30 rpm to produce a uniform solute concentration across the substrate surface at a thickness of 1-2 μm. Pure Al, an Al-19 $^{a}/_{o}$ Mo alloy, and an Al-26 $^{a}/_{o}$ W alloy, in both as-sputtered and heat treated (except for the pure Al) conditions were produced and characterized by XRD, anodic polarization, and galvanic coupling with graphite.

In order to evaluate the effects of heat treatment on corrosion performance, half of each Al-19 a/o Mo and Al-26 a/o W wafer were heat treated in the deposition chamber fitted with a hot stage. While the specimens were in the load lock, the stage was heated to 400 °C and allowed to stabilize. The specimens were then transferred into the chamber and heat treated for one hour before removal through load lock and air cooling. The heat treatment was conducted at 100 mTorr in flowing high purity argon gas.

Alloys were characterized using scanning electron microscopy (SEM), energy dispersive spectroscopy (EDS), X-ray diffraction (XRD), and optical microscopy. Alloy compositions were determined by EDS in three separate areas using semi-quantitative analysis of the X-ray spectra. XRD was conducted on each film to determine whether the solute elements were in solid solution with the Al after sputtering and following heat treating. Intensity versus diffraction angle (2θ) was measured for each alloy before and after heat treatment and plotted together for direct comparison of the effect of heat treatment on the thermal stability of the alloy. Before and after electrochemical testing, SEM and optical microscopy were used to observe surface features such as scratches, defects, pits, and cracks.

Electrochemical specimens were prepared by cleaving the silicon wafer into pieces approximately 1 cm x 1 cm. Following this, the alloy was attached to a lead wire, and the edges and back of the sample were painted with a marine epoxy (Interlux 404/414) so that only the alloy's surface was exposed to the electrolyte.

Anodic potentiodynamic polarization curves were generated using an EG&G Princeton Applied Research (PAR) Model 273 Potentiostat interfaced with an IBM PS/2 computer controlled by PAR Softcorr Corrosion Software (Model 352) at a scan rate of 0.2 mV/sec. A few experiments were conducted at slower scan rates (0.05 and 0.008 mV/sec) to confirm the breakdown potential. The experiments were conducted at ambient lab temperature in quiescent 0.1 M NaCl solution adjusted to a pH of 8 with NaOH. This pH was chosen because of interest in performance in marine environments The specimens were allowed to reach a steady state potential prior to polarization which took approximately one hour.

Amoco P75 graphite fibers (UTS=2.1 GPa, E=520 GPa) embedded in polyetheretherketone (PEEK) were used to perform polarization and galvanic couple experiments. Edges of the specimen (approximately 0.21 cm^2) were sanded to expose fibers to the electrolyte. Again, marine epoxy was used to isolate all but one sanded edge of the specimen. P75 graphite was cathodically polarized at a scan rate of 0.2 mV/sec, and the area was estimated by measuring the tested surface area and multiplying it by the fiber volume fraction (53.8 %) calculated with a Buehler Omnimet II Image Analyzer

The generated polarization data were then superimposed to form galvanic current diagrams which were used to estimate the effects of galvanic coupling on the corrosion rate of the Al and Al alloys Actual galvanic current

measurements were also taken for P75 graphite samples coupled to pure Al, Al-19 a/o Mo, and Al-26 a/o W specimens, in both as-sputtered and heat treated conditions. Cathode to anode area ratios (c:a) of approximately 0.15 and 0.40 were used to evaluate galvanic compatibility. The higher c:a ratio was chosen to approximately model the ratio found in a composite, while the lower value represents a less aggressive ratio. These specimens were tested in 0.1M NaCl (pH 8) for approximately 1 week. The currents were measured as a function of time using a bank of Zero Resistance Ammeters (ESC Model 440 Multichannel Potentiostat/Zero Resistance Ammeter).

RESULTS AND DISCUSSION

Immediately after removal from the sputtering system and after heat treatment at 400°C for 1 hour, surfaces of the Al-19 a/o Mo and Al-26 a/o W alloys were examined visually and found to be highly reflective with no cloudiness, which would indicate contaminants in the film. XRD spectra for the Al-26 a/o W alloy is presented in Figure 2. Ignoring the Si peaks at 33°, 70°, and 116°, there are two very broad peaks centered at approximately 21° and 41° indicative of an amorphous structure.[21-23] No changes were noted in the diffraction pattern after heat treatment. The Al-19 a/o Mo XRD pattern was almost identical to the data shown in Figure 2 for the Al-W alloy--broad peaks were observed at 21° and 41° and no changes were observed as a result of heat treatment. High resolution spectra for both alloys are shown in Figure 3. The peak centered at 21° appears to be an amorphous phase that has short range order similar to $Al_{12}Mo$ and Al_5Mo for the Mo alloy or $Al_{12}W$ and Al_5W for the W alloy. These phases have a number of planes which reflect over these angles. In a similar fashion, the broad peak centered at 41° may be more closely associated with the Al, Mo or W metals. These results indicate that the films had no crystalline structure, i.e., no long range order, and that the films may actually contain the precursors to Al-Mo or Al-W intermetallic compounds. Subsequent TEM bright-field and selected area diffraction analysis of the alloy films revealed no structure in the films, no diffraction of the beam in tilting, and two large amorphous rings at d values identical to the peaks found at 21° and 41°.

Table 1 presents all of the polarization data for the pure Al, Al-19 a/o Mo and Al-26 a/o W alloys. From this table it can be seen that replicate tests were fairly reproducible. The largest variation among all of the tests was 55mV for the corrosion potential and 150 mV for the breakdown potential (both for the as-sputtered Al-19 a/o Mo data). With the exception of two experiments, the values of the passive current densities were relatively close to each other and similar to that of pure Al. Some of the variations from specimen to specimen may have been caused by very small defects in the film resulting from dust particles on the substrate prior to alloy deposition. One such suspected site is shown in Figure 4.

Figure 5 shows the anodic polarization behavior for the as-sputtered pure Al, and the Al-19 a/o Mo and Al-26 a/o W alloys. As has been reported in the past, dramatic improvements in the breakdown potentials were noted for the

nonequilibrium alloys, and both show more noble corrosion potentials than pure Al. The Al-Mo alloy exhibits an average corrosion potential of -515 mV_{SCE} which is 510 mV higher than the pure Al and 215 mV higher than the Al-W. An average breakdown potential of 535 mV_{SCE} was noted for the Al-W which is 1245 mV higher than the average for pure Al and 140 mV higher than the average for Al-Mo. Similar passive current densities were observed for the two alloys and for pure Al. These similarities combined with information on the passive film chemistries for Al-W and Al-Mo alloys suggests that the modified alloy passive films may be closer in composition to the film which forms on pure Al than those which form on either pure W or pure Mo.[24]

The breakdown potential shown in Figure 5 for the Al-26 a/o W alloy is significantly lower than the breakdown potential for the Al-10a/o W alloy found earlier by Shaw et al.[15] These differences are believed to be related to the conditions under which the alloys were deposited. For the alloys shown in Figure 1, the sputtering system was located in a class 100 clean room, whereas, for the alloys shown in Figure 5, the sputtering system was located in a lab environment. Dust particles on the substrate surface prior to deposition could affect the growth of the film, resulting in lower breakdown potentials. The breakdown potentials reported for the alloys produced in the lab environment still represent a dramatic improvement in corrosion performance over pure Al and are indicative of the operating conditions that will be present when actual fibers are sputter coated.

The most encouraging attribute of these alloys is that they retain their enhanced corrosion behavior after heat treating at 400 °C for 1 hour as shown in Figures 6 and 7. This excellent performance is attributed to the amorphous structure which is maintained even after heat treatment. Enhanced corrosion resistance at an elevated temperature is essential for fabrication, because the coated fibers will need to be HIP'ed. These high concentration Al-Mo and Al-W alloys show outstanding polarization behavior after heat treating which was not observed by Shaw et al. for the lower solute concentration alloys.[15] The Al-1.5a/o W and Al-5a/o W alloys in their research contained precipitates after heat treating for 1 hour at 400 °C and showed 90 to 800 mV decreases in the breakdown potential, respectively.

A galvanic current diagram for P75 graphite coupled to pure Al and Al-19 a/o Mo (as-sputtered) is presented in Figure 8. In the case of pure Al, the cathodic, current limited, oxygen reduction reaction for graphite crosses the Al anodic reaction in the pitting region where high galvanic currents are expected. In the case of the Al-19 a/o Mo, the cathodic, oxygen reduction reaction crosses the alloy's anodic curve in the passive region where low galvanic corrosion current for the matrix metal is predicted. Considering similar cathode-to-anode area ratios, the pure Al/Gr couple would have an estimated galvanic corrosion current of 141 μA (141 $\mu A/cm^2$) while the predicted galvanic corrosion current of the Al-19 a/o Mo/Gr couple is 0.93 μA. Therefore, the enhanced passive region for the alloy results in a significantly lower galvanic current. The Al-Mo heat treated alloy showed similar behavior since the polarization results were identical to the as-sputtered sample.

The Al-26 $^{a}/_{o}$ W/Gr galvanic current diagram is shown in Figure 9. Again, the enhanced passivity of the alloy causes the galvanic corrosion current of the couple to decrease from 141 μA for the pure Al/Gr to 0.63 μA for the Al-W/Gr couple. Heat treated Al-W would show identical behavior due to the similarity of its polarization response to the as-sputtered alloys.

Long-term galvanic current measurements were taken to confirm the predictions made using galvanic current diagrams, and two alloys from each sample were tested to verify the results. Figure 10 shows the galvanic current versus time data for the as-sputtered pure Al, and the as-sputtered and heat treated Al-19 $^{a}/_{o}$ Mo and the Al-26 $^{a}/_{o}$ W each coupled to P75 graphite in 0.1M NaCl at pH 8 for 7 days. The pure Al/Gr couple (c:a=0.11) had an initial galvanic corrosion current of 40μA that dropped off to a value of 10.9μA (corresponding to a current density of 5.5 μA/cm^2) after 7 days. Visual observations revealed that very little Al was still present on the Si substrate. The other Al/Gr couple had a cathode to anode area ratio of 0.13 and exhibited similar behavior.

The cathode-to-anode area ratio for the Al-19 $^{a}/_{o}$ Mo/Gr couple was 0.41. A current of approximately 3 μA was initially observed, which subsequently decreased to 0.1 μA after 1 hour. After 16 hours, the current dropped to a steady state value of 0.05 μA (corresponding to a current density of 0.16 μA/cm^2) and remained constant for the duration of the experiment. The other Al-Mo/Gr couple (c:a=0.15) came to a steady state of 0.06 μA (i = 0.09 μA/cm^2) for the first 3 days, then increased to approximately 8 μA for the remaining time. After the experiments, the surfaces of both alloys appeared reflective with no evidence of pitting. SEM of this specimen revealed that the coating was still present and in good condition after testing. The increase in current on the second sample is believed to have been caused by a small flaw in the coating or a scratch in the film which initially did not extend to the substrate. The galvanic current densities after several days of testing were slightly lower than the values predicted by the galvanic current diagram (0.16 μA/cm^2 vs. 0.28μA/cm^2) which shows that the diagrams provide a reasonably good estimate of the actual galvanic behavior.

The Al-W alloy/Gr couple (c:a=0.43) had an initial current of 12.4 μA which fell to a value of 0.7 μA (i = 2.1 μA/cm^2) for the next 35 hours before gradually increasing to a value of 3.2 μA (corresponding to a current density of 9.6 μA/cm^2) at the end of the 7 day test. The other galvanic couple for this alloy with a cathode to anode area ratio of 0.16 exhibited similar behavior. After testing, the surfaces of both specimens were reflective and no evidence of pitting was observed. Again, it is believed that small flaws or scratches may have lead to the increase in current after a few days of exposure.

The heat treated alloys also had low steady state galvanic corrosion currents. An initial current of 6.1 μA was noted for one of the two Al-19 a/o Mo heat treated/P75 graphite couples (c:a=0.14) which dropped off to a steady state value of 1.5 μA (1.6 μA/cm^2) after approximately 6 days. The second couple with a cathode to anode area ratio of 0.18 also showed an initial current of 6.1 μA which fell off to a value of 2.4 μA after 45 minutes and then decreased to 0.16 μA after 50 hours. Following this, the current for the second couple increased to 9 μA (i = 12.6 μA/cm^2) and occasionally oscillated between anodic and cathodic behavior. At the end of the test, it was noted that the second specimen contained a small blistered region near the top of the specimen. The remaining 70% of this specimen was intact and in good condition with no pits. After testing, the first specimen was found to be fully intact, optically reflective, and free of pits.

The data for one of the two heat treated Al-26 a/o W alloy/Gr couples (c:a=0.43) had an initial current of 16 μA which fell to a steady state value of 0.05 μA (corresponding to a current density of 0.1 μA/cm^2) for the remainder of the experiment. The second heat treated Al-W alloy/Gr couple with a cathode to anode area ratio of 0.16 exhibited an initial current of 1 μA and a steady state value of 0.3 μA (i = 0.33 μA/cm^2). After testing, the surfaces of both alloys were reflective and no evidence of pitting was observed.

While the nature of the specimens appears to make determination of an exact steady state galvanic current difficult in some cases, the important issue of whether or not the performance of a composite could be improved through nonequilibrium alloying is easily answered by the visual appearance of the specimens after testing. Comparing the appearance of the surfaces of pure Al, the Al-19 a/o Mo alloy, the Al-26 a/o W alloy, and the heat treated Al-26 a/o W alloy after galvanic coupling to graphite for 1 week, the alloy surfaces were optically reflective after testing, while only a small amount of the pure Al film remained after the 7 days.

Al-Mo and Al-W alloys containing more than 10a/o solute were heat treated at nominal consolidation temperatures and retained their corrosion resistance. XRD results show no evidence of a change in the diffraction pattern after heat treating. Below 10a/o solute, the films can not be heat treated without the solute reacting to form Al intermetallic phases, which degrade the corrosion performance.[20]

CONCLUSIONS

Co-sputter deposited Al-19 a/o Mo and the Al-26 a/o W nonequilibrium alloys show superior corrosion behavior over pure Al. Heat treatment of these alloys at 400 °C for 1 hour did not result in the precipitation of a second phase and the performance of these alloys in both polarization experiments and galvanic tests was equivalent to that of as-sputtered alloys. Galvanic current diagrams show that the alloys have much lower galvanic corrosion currents

than the pure Al which is a result of their enhanced passivity. Long-term galvanic corrosion experiments revealed essentially no degradation for either of the alloys; whereas, corrosion penetrated the pure Al film, exposing the Si substrate after just several days.

ACKNOWLEDGEMENTS

The authors would like to thank Ed Principe and Paul Miller for the SEM micrograph of the breakdown site. This program was funded by A.J. Sedriks of the Office of Naval Research under contract number N00014-91-J-1196.

REFERENCES

1. M. M. Aylor and R. M. Kain, ASTM STP 864 - Recent Advances in Composites in the US and Japan, Vinson and Taya (editors), American Society for Testing and Materials, Philadelphia, p 632 (1985).

2. W. H. Pfeifer, W. J. Renton (editor), American Institute of Aeronautics and Astronautics, New York, 231 (1977).

3. M. G. Vassilaros, D. A. Davis, G. L. Steckel, and J. P. Gudas, Proceedings of the 1980 Tri-Service Corrosion Conference, Vol. 2, US Government Publication, 21 (1980).

4. D. M. Aylor, R. J. Ferrara, and R. M. Kain, *Mater. Perf.*, **23**, 32 (1984).

5. D. M. Aylor and P. J. Moran, *J. Electrochem. Soc.*, **132**, 1277 (1985).

6. D. L. Dull, W. C. Harrigan, Jr., and M. F. Amateau, Aerospace Report ATR-76 (7564)-1, California (1977).

7. E. G. Kendall and D. L. Dull, National Technical Information Service, U.S. Department of Commerce, AD-777, 160 (1974).

8. L. H. Hihara, Ph.D. Dissertation, Massachusetts Institute of Technology, Cambridge, MA (1989).

9. C. R. Crowe, NRL Memorandum Report 5415, Naval Research Laboratory, Washington, DC (1985).

10. W. C. Moshier, G. D. Davis, J. S. Ahearn, and H. F. Hough, *J. Electrochem. Soc.*, **133**, 1063 (1986).

11. Ibid, **134**, 2677 (1987).

12. W. C. Moshier, G. D. Davis, and G. O. Cote, *ibid.* **136**, 356 (1989).

13. G. D. Davis, W. C. Moshier, T. L. Fritz, and G. O. Cote, *ibid.* **137**, 422 (1990).

14. B. A. Shaw, T. L. Fritz, G. D. Davis, and W. C. Moshier, *ibid.* **137**, 1317 (1990).

15. B. A. Shaw, G. D. Davis, T. L. Fritz, B. J. Rees, and W. C. Moshier, *ibid.* **138**, 3288 (1991).

16. D. C. Bennett, M.S. Thesis, University of Connecticut, Storrs, CT (1972).

17. H. P. Hack and J. R. Scully, *Corrosion*, **42** (2), 79 (1986).

18. D. A. Jones, *Corrosion*, **40** (4), 181 (1984).

19. G. S. Frankel, M. A. Russak, C. V. Jahnes, M. Mirzamaani, and V. A. Brusic, *J. Electrochem. Soc.*, **136**, 1243 (1989).

20. B. A. Shaw, T. R. Schrecengost, W. C. Moshier, and R. G. Wendt, Martin Marietta Space Systems Annual Report, ONR-TPSU-MMC-1196-693, "Inhibiting Corrosion in Gr/Al and Gr/Mg MMCs Using Nonequilibrium Alloying Techniques", (1992).

21. P. Furrer and H. Warlimont, "Crystalline and Amorphous Structures of Rapidly Solidified Al-Cr Alloys", *Mater. Sci. E.*, **28**, 127 (1977).

22. K. Asami, H. Yoshioka, K. Hashimoto, K. Shimizu, and K. Kobayashi, "Superlattice-Like Structure of Sputter-Deposited Amorphous Aluminum-Heavy Element Alloys", *J. Non-Crys. Solids*, **110**, 258 (1989).

23. Y. He, S. J. Poon, and G. J. Shiflet, "Synthesis and Properties of Metallic Glasses That Contain Aluminum", *Science*, **241**, 1640 (1988).

24. G. D. Davis, B. A. Shaw, B. J. Rees, and M. Ferry, *J. Electrochem. Soc.*, **140** (4), 951 (1993)

Table 1. Anodic polarization data for the pure Al, Al-19.1 Mo, and Al-25.9 W in 0.1M NaCl at pH 8 (HT = heat treated, ** = average)

SAMPLE	SCAN (mV/s)	Ecorr (mV-SCE)	Eb (mV-SCE)	ipass (μA/cm)
Al	0.2	-1070	-720	0.18
Al	0.2	-980	-700	0.05
Al - 19.1 Mo	0.2	-490	320	1.26
Al - 19.1 Mo	0.2	-545	470	1.26
Al - 19.1 Mo (HT)	0.2	-565	400	9.52
Al - 19.1 Mo (HT)	0.2	- - -	410	0.50
Al - 19.1 Mo (HT)	0.2	-595	445	1.00
Al - 19.1 Mo (HT)	0.05	-590	440	1.00
Al - 19.1 Mo (HT)	0.008	-560	400	0.60**
Al - 25.9 W	0.2	-700	500	4.50**
Al - 25.9 W	0.2	-745	550	0.63
Al - 25.9 W	0.2	-740	550	0.63
Al - 25.9 W (HT)	0.2	-775	550	0.63
Al - 25.9 W (HT)	0.2	-775	545	0.63

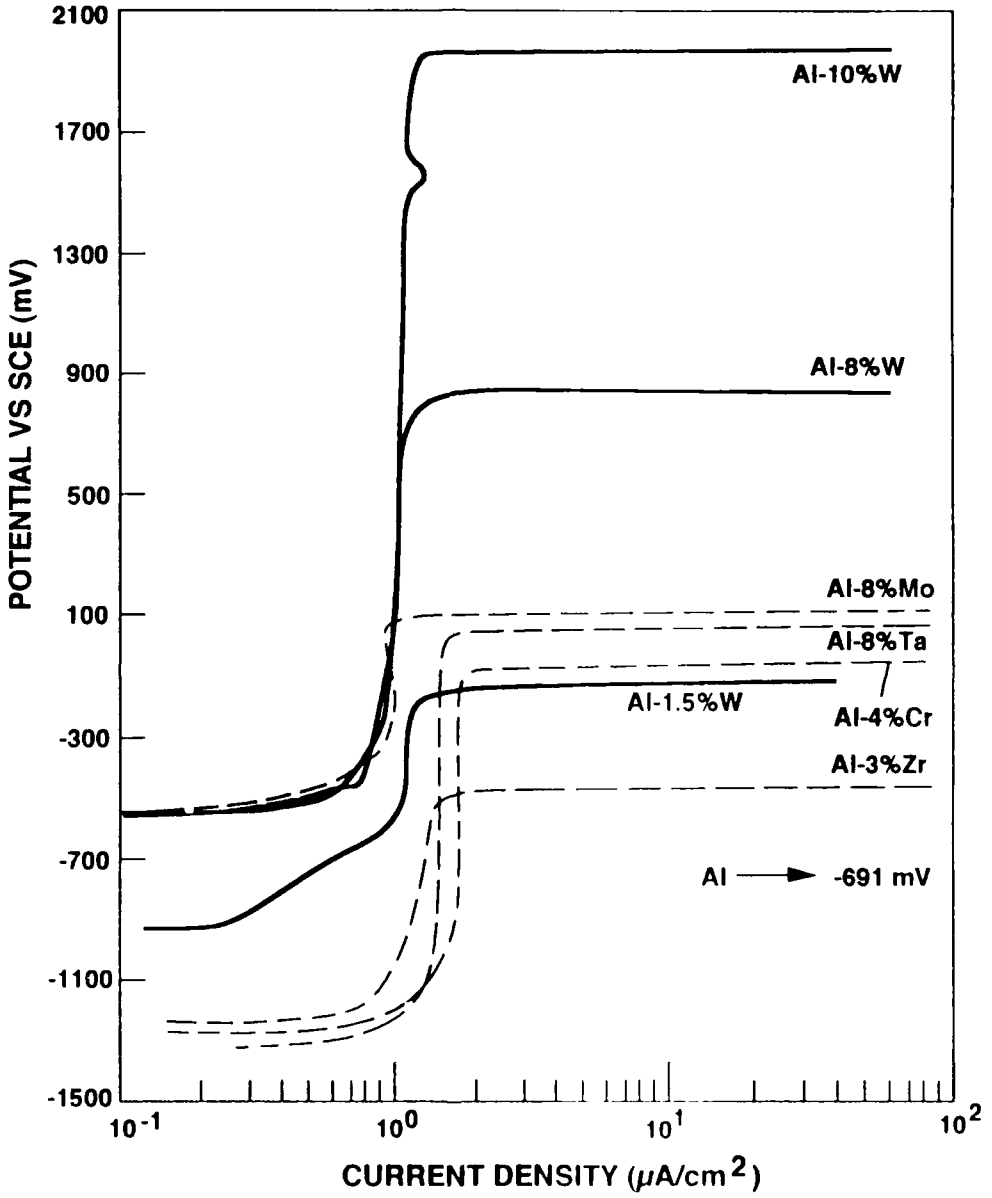

Figure 1. Anodic polarization behavior for a variety of nonequilibrium Al alloys in aerated 0 1M KCl compared to the spontaneous pitting potential of pure Al (-691mV vs SCE) at 0 167 mV/sec Source Shaw et al , *J Electrochem Soc* 138 3288 (1991)

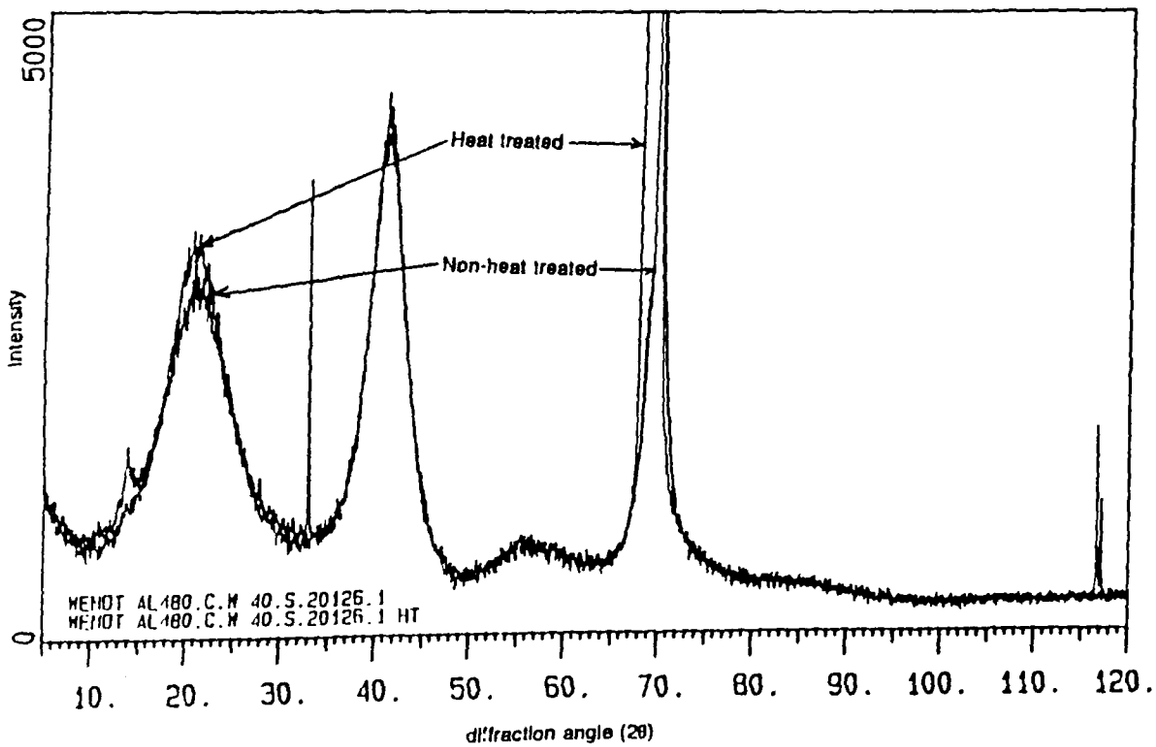

Figure 2. XRD patterns for Al-25.9 W before and after heat treatment

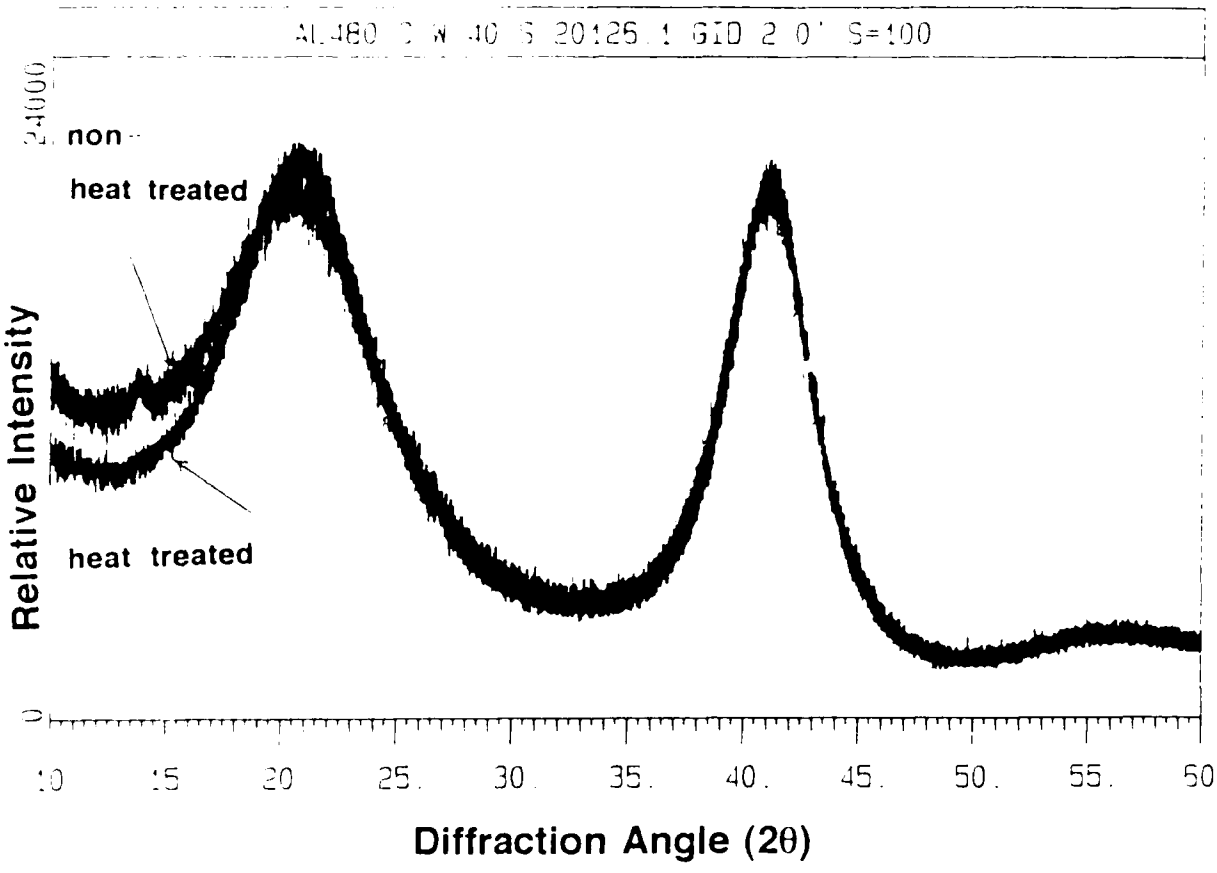

Figure 3 a High resolution X-ray diffraction pattern for the 26 $^{a}/_{o}$ W alloy showing broad amorphous peaks at 21° and 41°

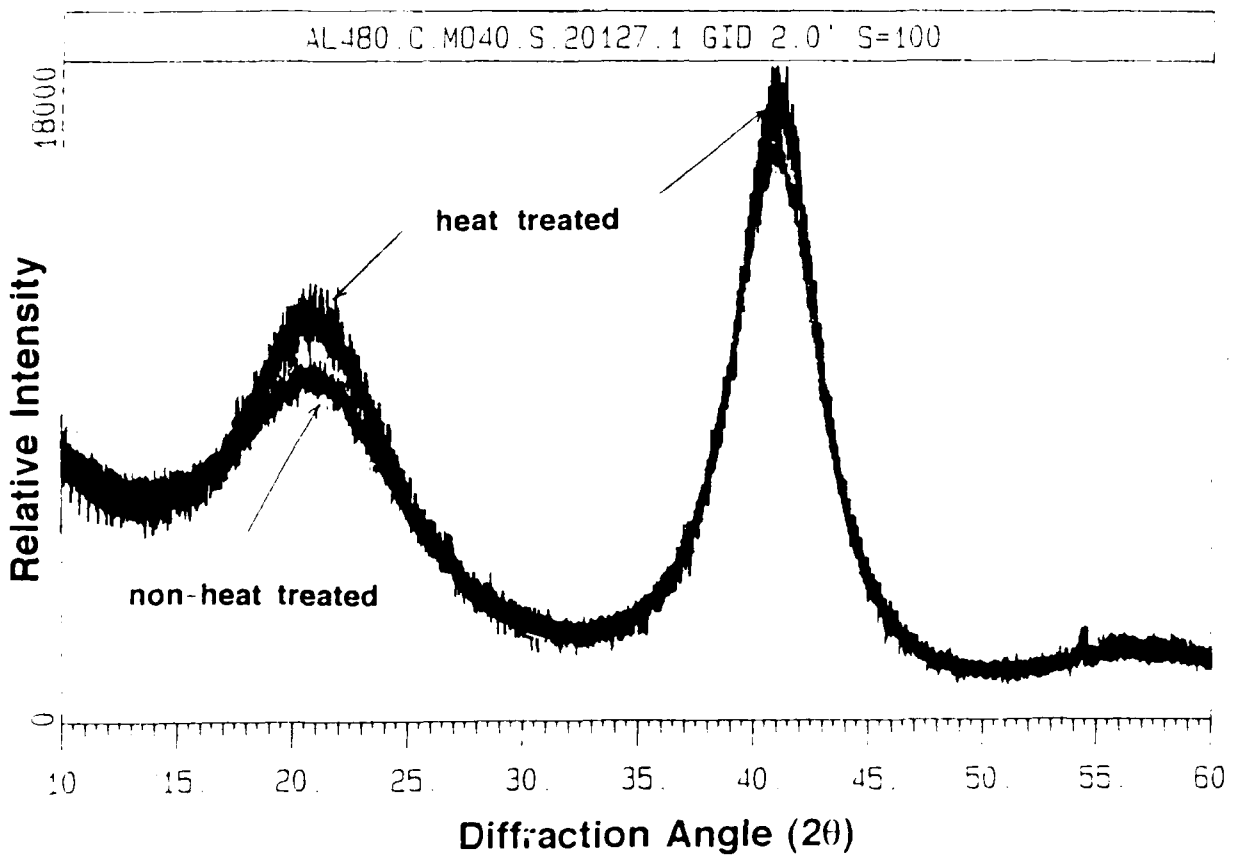

Figure 3 b High resolution X-ray diffraction pattern for the 19 a/o Mo alloy showing broad amorphous peaks at 21° and 41°

Figure 4 SEM micrograph of a breakdown site on an Al-Si specimen that appears to have initiated as a result of a dust particle on the Si surface

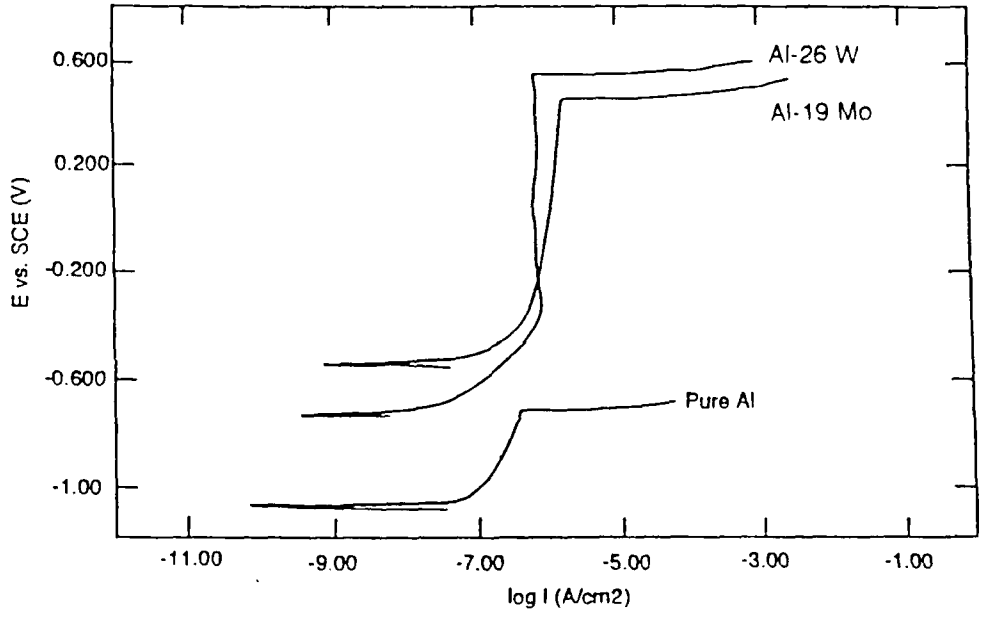

Figure 5 Anodic polarization behavior of Al-19.1 Mo and Al-25.9 W in 0.1M NaCl at pH 8 at 0.2 mV/sec compared to pure Al

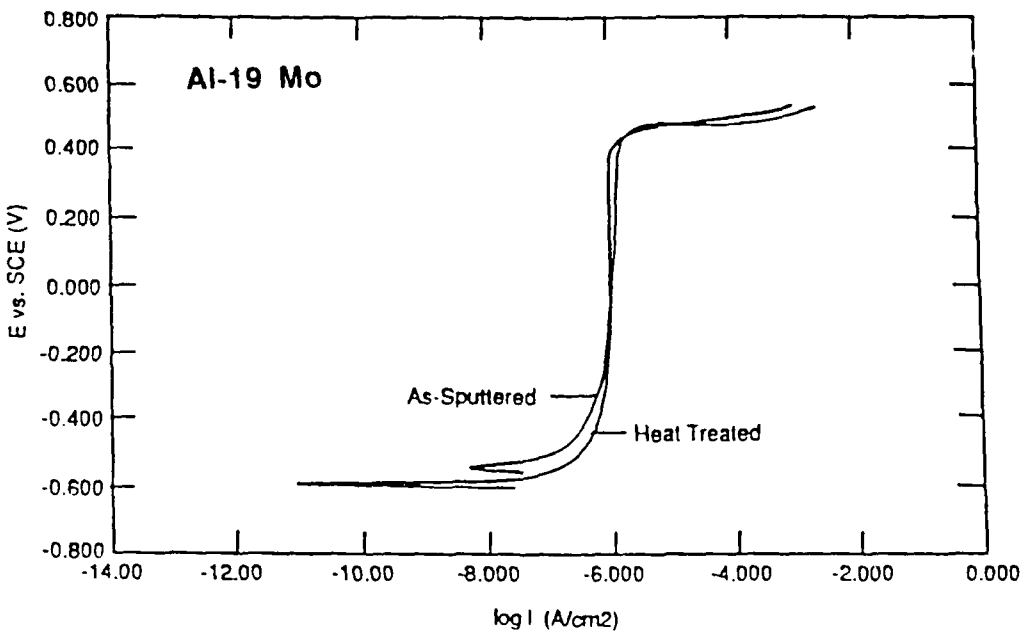

Figure 6 Anodic polarization behavior of Al-19.1 Mo (as-sputtered vs. heat treated) in 0.1M NaCl at pH 8 at 0.2 mV/sec

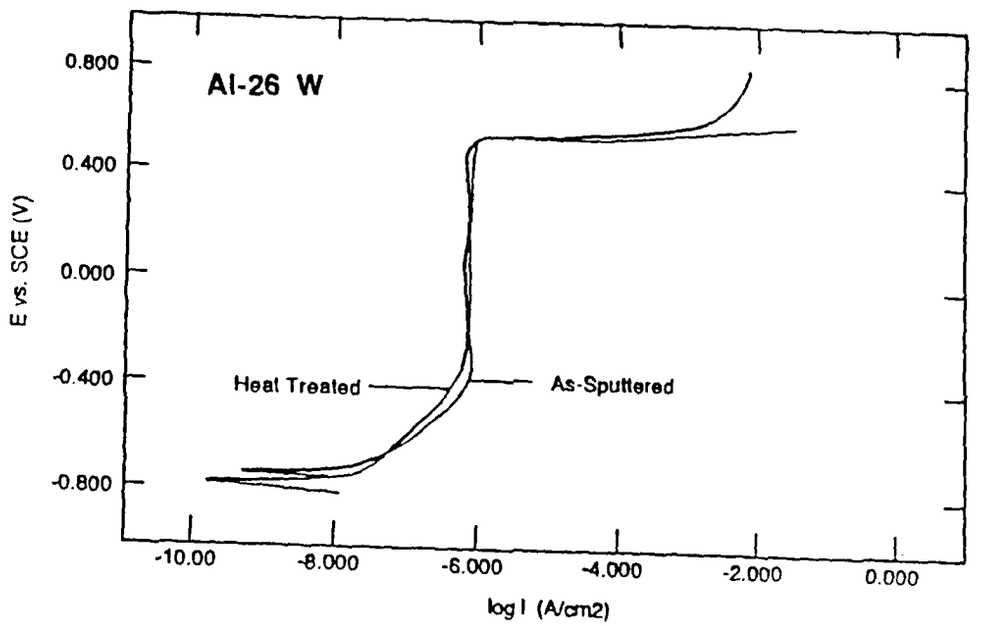

Figure 7 Anodic polarization behavior of Al-25.9 W (as-sputtered vs. heat treated) in 0.1M NaCl at pH 8 at 0.2 mV/sec

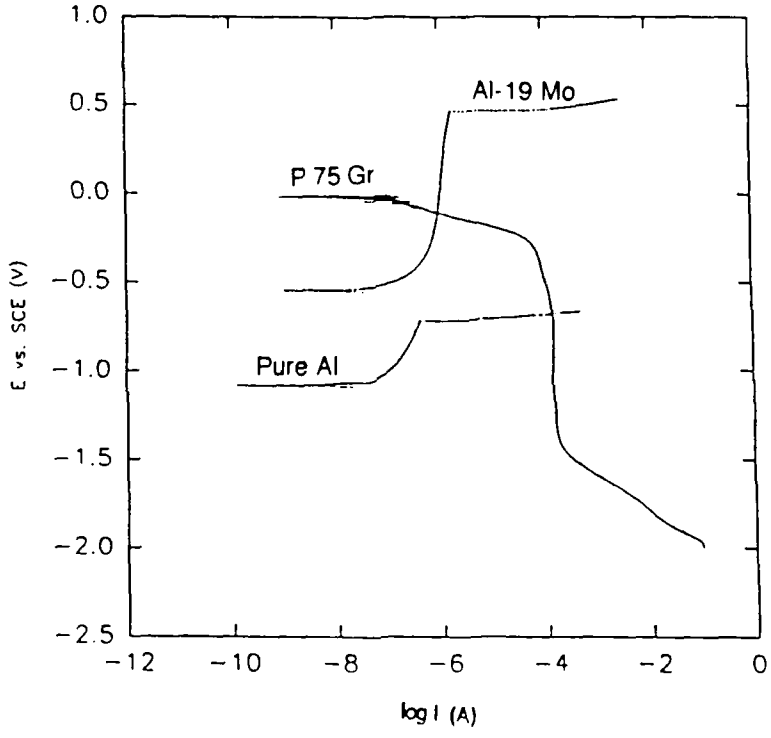

Figure 8 Galvanic current diagram for P75 graphite coupled to pure Al and Al-19.1 Mo in 0 1M NaCl at pH 8 at 0.2 mV/sec (assuming cathode to anode area ratio equals one)

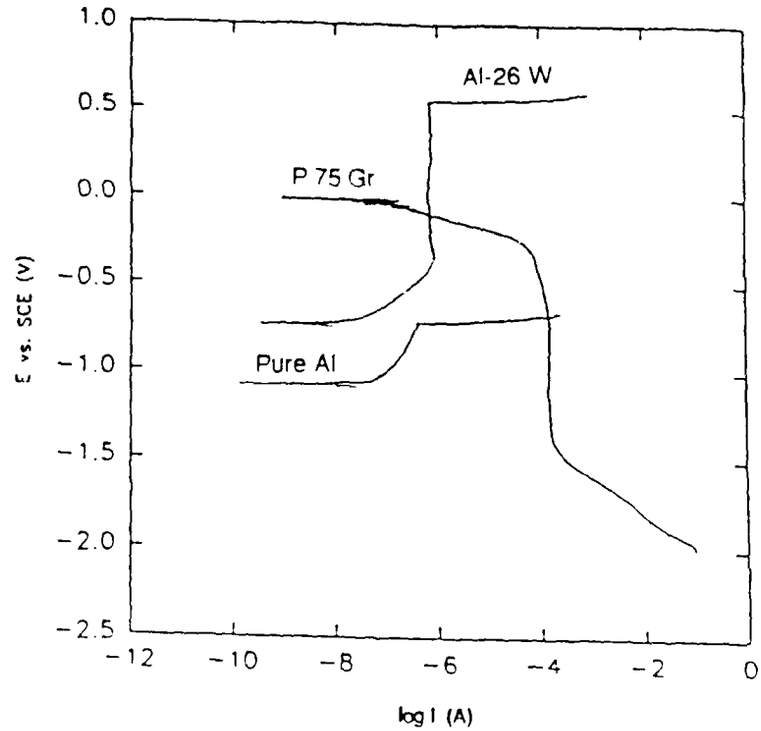

Figure 9 Galvanic current diagram for P75 graphite coupled to pure Al and Al-25 9 W in 0.1M NaCl at pH 8 at 0 2 mV/sec (assuming cathode to anode area ratio equals one)

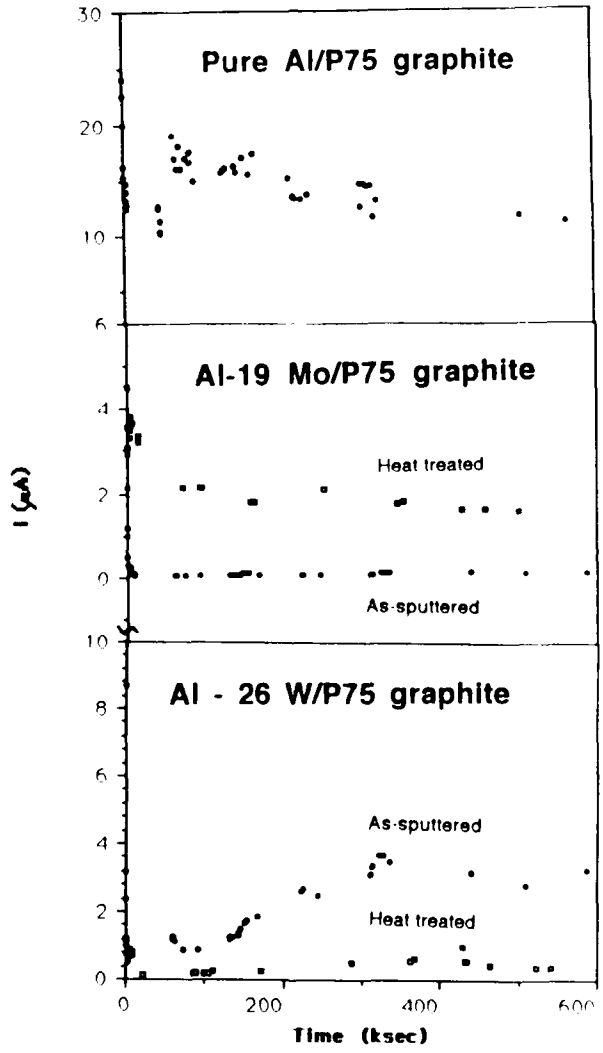

Figure 10 Galvanic current vs time for the as-sputtered pure Al/Gr, and the as-sputtered and heat treated Al-19 1 Mo/Gr and Al-25 9 W/Gr couples in 0 1M NaCl at pH 8 for 7 days (cathode to anode area ratios are 0 11, 0 41, 0 14, 0 14,and 0 43, respectively)

Appendix 3

Corrosion Resistant Aluminum Matrix for Graphite/Aluminum Composites

R.G. Wendt, W.C. Moshier, B.A. Shaw and P.L. Miller

(submitted to Corrosion June 1993)

Corrosion Resistant Aluminum Matrix for Graphite/Aluminum Composites

R.G. Wendt and W.C. Moshier
Martin Marietta Astronautics Group
Denver, CO 80127

B.A. Shaw and P.L. Miller
Pennsylvania State University
University Park, PA 16802

ABSTRACT

Corrosion resistant Al matrix alloys for graphite fiber reinforced Al (Gr/Al) composites have been developed by alloying with Mo via magnetron sputtering. Galvanic corrosion of the Al-Mo alloys coupled to equal areas of P75 graphite (Gr) fibers was limited by the anodic reaction as a result of the alloys high open circuit potential (E_{oc}) combined with a positive breakdown potential (E_b). Heat treating to nominal Gr/Al composite consolidation temperatures had little impact on the galvanic corrosion behavior and the attack remained anodically controlled.

Aluminum alloys were sputtered with concentrations ranging from 4 to 26 atomic percent (at. %) molybdenum. Most of the alloys had an amorphous structure in the as-deposited condition as determined by x-ray diffraction (XRD). The measured open circuit potential from polarization experiments for the Al-Mo alloys averaged approximately -550 mV_{SCE} (referenced to a saturated calomel electrode, SCE) when tested in quiescent 0.1 M NaCl, pH 8 and was not found to be a function of Mo concentration. Breakdown potential values varied from 100 mV_{SCE} for Al-4Mo to 750 mV_{SCE} for Al-26Mo.

Many of the alloys were heat treated at 400, 500, and 600°C for 1, 2, and 8h to assess the effect of nominal composite consolidation temperatures on the alloy structure and corrosion behavior. XRD of the alloys with low Mo concentrations (Al-4Mo and Al-11Mo) showed several phases had precipitated after a heat treatment to only 400°C for 1 h, which is the lower bound for consolidating a Gr/Al composite. However, Al-23 Mo alloys could be heat treated to 600°C for up to 8 h, without evidence of precipitation.

After heat treatment, the alloys still had an open circuit potential more noble than the breakdown potential of pure Al and each alloy exhibited a passive region that extended to positive potentials relative to the SCE. For example, an E_{oc} of -556 mV_{SCE}, E_b of 335 mV_{SCE} and passive current density (i_{pass}) of 0.38 $\mu A/cm^2$ in a quiescent 0.1 M NaCl, pH 8 solution was measured for Al-18Mo heat treated at 400°C for 8 h. These values are very similar to the as-deposited Al-18Mo alloys and are a significant improvement over pure Al (E_{oc} = -1662 mV_{SCE}, and E_b = -691 mV_{SCE}) tested in the same environment.

Measured galvanic currents for as-deposited Al-18Mo and Al-23Mo alloys coupled to equal areas of P75 Gr were 0.04 to 0.08 μA (0.04 to 0.08 $\mu A/cm^2$), respectively, which are

3 orders of magnitude lower than pure Al which exhibited average galvanic current values of up to 30 μA (30 μA/cm^2)in quiescent 0 1 M NaCl, pH 8 solution when coupled to P75 graphite fibers Similar tests conducted on Al-18Mo after several different thermal aging treatments showed the galvanic current was at least an order of magnitude lower than that of pure Al Galvanic current diagrams indicated corrosion was controlled by the anodic reaction Changing the area ratio shifts the cathodic curve to higher passive current values but the galvanic reaction remained under anodic control Therefore, the corrosion resistance of Al-Mo alloys should not be affected by changes in the graphite fiber volume fraction

1.0 INTRODUCTION

High modulus Gr/Al metal matrix composites (MMCs) offer a wide variety of attractive properties including high specific modulus and strength (E/ρ and UTS/ρ), tailorable or zero coefficient of thermal expansion (CTE), and high thermal conductivity (K) These properties are ideal for designing mechanically (E/ρ) and thermally (α/K) stable structures However, Gr/Al is very susceptible to corrosion, which has limited its application in aircraft, spacecraft, and marine structures

A study of the corrosion of Gr/Al showed that composites corroded at rates up to eighty times faster than monolithic Al alloys in an aerated 3 15 wt % NaCl solution at room temperature [Ref 1] One of the key factors behind the rapid corrosion of Gr/Al composites is residual microstructural chlorides introduced during the liquid metal infiltration process for fabricating precursor Gr/Al wires [Ref 1-7] Corrosion of Gr/Al composite initiates by pitting of the facesheet foils at a rate commensurate with Al alloys Once these foils have been penetrated, corrosion is accelerated by residual microstructural chlorides within the composite and by exposure of the Gr fibers creating a galvanic couple with the Al matrix [Ref 4]

To improve the corrosion resistance of Gr/Al metal matrix composites, several techniques such as coatings, cathodic protection, and the use of cathodic inhibitors, have been investigated [Ref 1-7] However, these protection techniques often adversely affect composite properties and only delay pitting and subsequent galvanic interaction between the Al matrix and fiber In addition, none of these techniques addresses the true problem, which is poor corrosion resistance of the Al matrix in chloride environments, especially when the metal is coupled to more noble graphite

An alternate process for preparing Gr/Al composites is by depositing the Al matrix directly onto each individual Gr fiber by physical vapor deposition (PVD) The versatility of the PVD process allows for virtually any matrix alloy to be deposited on the Gr fibers Sputtering of metal alloys onto Gr fibers has several potential advantages over the liquid metal infiltration process used to fabricate Gr/Al composites, including 1) elimination of fiber/matrix reaction because the composites can be consolidated well below the melting point of Al where the kinetics for aluminum carbide formation are sluggish, 2) minimization of thermal strain hysteresis due to the high strength of the sputtered alloy matrix, 3) providing near-net shape processing capability [Ref 8 9] and 4) elimination of residual microstructural chlorides

Combining nonequilibrium Al-Mo and Al-W alloys developed and characterized earlier [Ref 10-18] with Gr/Al composites provides a practical application to the sputtering

technique of fabricating Al alloys while potentially improving the poor corrosion resistance associated with Gr/Al. Al alloyed with 5 to 25 at. % Mo and W were fabricated and corrosion tests showed a positive breakdown potential even after heat treating to 400°C for 1h [Ref 19]. The sputtering process does not introduce residual chlorides as in the liquid metal infiltration process, further improving the composites' inherent corrosion performance. Transition into commercial practice only requires incorporation of these new alloys as the sputtering target material and establishing the consolidation parameters for the new alloy.

The objective of this work was to lay the ground work for using nonequilibrium sputtered Al alloys as the matrix for Gr/Al composites. The major emphasis was to determine whether the enhanced corrosion behavior provided by nonequilibrium alloying could be maintained after heat treating to typical composite consolidation temperatures. In addition, experiments to determine the galvanic corrosion behavior of the nonequilibrium alloys coupled with P75 graphite fibers were conducted. Lastly, although significant increases in the breakdown potential can be achieved by alloying with either tungsten or molybdenum, the density of the Al alloy also significantly increases. Therefore, this work focuses on Mo, the lower density solute, and also investigates the addition of magnesium to form ternary Al-Mg-Mo alloys to see whether the positive breakdown potentials could be achieved and maintained after heat treatment.

2.0 EXPERIMENTAL PROCEDURE

Binary Al-Mo and ternary Al-Mg-Mo alloys were prepared by sputtering the respective elements from high purity targets onto 100 mm diameter single crystal Si or sapphire wafers to a thickness of 1 μm. Substrate temperature was not controlled during sputtering, and reached a maximum temperature of approximately 100°C during a 1 h deposition. Composition of each alloy was varied by holding the Al target at a constant power of 485 watts (W RF) while the power for the Mo and Mg cathodes were varied between 10 to 100 W DC. Pressure was held constant at 7.0 mtorr during sputtering by introducing purified (<10 ppb O_2) Ar gas at a flow rate of 200 standard cubic centimeters per minute (SCCM) and adjusting the conductance of the system. The vacuum system consisted of a CTI Cyrotorr 8 cyrogenic pump backed up with a Alcatel 100 diaphram/turbomolecular pump. This pump combination allowed the chamber to be pumped without the possibility of oil backstreaming into the process chamber. By spacing the sputtering heads approximately 100-mm (4-in) from the substrate focused at 60° from the substrate normal and rotating the substrate at 30 RPM, alloy composition uniformity could be maintained to within a few atomic percent solute across the 100 mm diameter substrate wafer.

Composition of the sputtered alloys was measured using a semi-quantitative computer program that analyzes the number of counts of elements in an energy dispersive spectrum (EDS) on a scanning electron microscope (SEM). Composition of several specimens were also measured by inductively coupled plasma (ICP) for comparison.

X-ray diffraction (XRD) was conducted on each alloy using a Rigaku Rotoflex 12 kW rotating anode diffractometer using a monochromatic Cu-K_α x-ray source. Intensity versus diffraction angle (2θ) was measured for each alloy before and after heat treating and plotted together for direct comparison of the effect of heat treatment.

Polarization specimens were fabricated by sectioning 100-mm-dia Si wafers coated with approximately 1 μm of alloy into several 1 cm^2 pieces. Leads were attached to the alloy using alligator clips and the continuity verified using a multimeter. The leads and specimens were then coated with a marine epoxy leaving an exposed alloy area of a little under 1 cm^2. The specimens were immersed into the electrolyte and tested using a standard three electrode technique. At least two replicate specimens were tested for each alloy and electrolyte. For most of the experiments, anodic polarization tests were conducted at ambient pressure and temperature in a quiescent 0.1M NaCl solution adjusted to pH 8 using reagent grade NaOH. Once the best alloy was identified, additional polarization tests were conducted in 0.1 M and 0.55 M NaCl (3.15 wt %) electrolytes in both the aerated and quiescent state. After immersion in the electrolyte, the specimens were allowed to reach a steady state open circuit potential which usually took approximately 1 h. The alloys were then polarized using a EG&G PAR *Model* 273 potentiostat/galvanostat starting at 10 mV_{SCE} more negative than the open circuit potential (E_{OC}) at a rate of 0.2 mV/s until breakdown occurred.

Galvanic corrosion response of the Al-Mo and Al-Mg-Mo alloys was estimated using galvanic current diagrams [Ref. 20]. In these diagrams, the anodic data for the Al-Mo alloys and pure sputtered Al were superimposed on the cathodic curve for P75 Gr fiber. Assuming the IR drop between the metal and graphite was insignificant, no contributions from reverse reactions, and uniform current distribution, the intersection of the anodic and cathodic curves was used to estimate the current present in the galvanic couple.

In addition, the galvanic current was measured by coupling ~1 cm^2 alloy specimens to P75 Gr fibers. These fibers were electrically connected to a lead and embedded in a nonconductive epoxy. The Gr fiber epoxy specimens were polished and probed with a multimeter to ensure that electrical continuity between the galvanostat lead and graphite fibers was maintained along the entire surface. The area fraction of graphite on the cathode surface was measured using a Buehler Omnimet II Image Analyzer. Final cathode-to-anode area ratios ranged from 0.2 for the as-deposited alloys to 1.1 for the heat-treated specimens. The alloy specimen and the P75 Gr/epoxy composite were electrically coupled and immersed in a pH 8, 0.1 M NaCl solution. Galvanic current was monitored as a function of time using an ESC Model 440 multichannel potentiostat/zero resistance ammeter (operating in the ZRA mode).

Alloy densities were predicted by assuming Mo atoms were in solid solution in the Al lattice. These predicted densities were compared to measured values determined by measuring the weight of alloy films of known thicknesses.

3.0 RESULTS

3.1 Alloy Fabrication and Heat Treatment

Compositions of the sputtered aluminum alloys with 4 to 26 at. % Mo are listed Table 1. All the as-sputtered alloys had a highly reflective metallic appearance after sputtering indicating low levels of contamination. After heat treating, most of the alloys retained their highly reflective appearance. In a few cases, the alloy either yellowed slightly or turned fluorescent blue. The Al-23Mo alloy fractured and spalled from the Si

wafer during cooling from the heat treatment temperatures, which gave erratic polarization results.

Several ternary alloys containing Mg were deposited onto polished single crystal sapphire wafers. These substrates were used to eliminate the reaction between the Si and the Mg that had occurred for Al-Mg-Mo alloys deposited on Si wafers. $MgSi_2$ formed rapidly, even at the lowest temperature (400°C) and shortest time (1 h), which resulted in a reaction consuming the Mg from the alloy and causing the film to fracture and delaminate from the Si wafer. Unfortunately, the Al-Mg-Mo alloys also reacted with the sapphire substrate to form oxides. Although the reaction was less extensive, it made it more difficult to resolve information in the XRD patterns.

3.2 X-ray Diffraction

XRD was conducted on both as-sputtered and heat treated Al-Mo alloys to determine whether the Mo (1) was in solid solution in the Al and readily available for incorporation into the passive film or (2) had reacted with Al to form Al_xMo_y intermetallic compounds during the sputtering process. In contrast to previous studies [Ref 10-17] aluminum peaks shifted to slightly higher 2θ values were not found. To delineate the onset of precipitation as a function of solute concentration, Al-11Mo, Al-18Mo, Al-23Mo binary alloys and an Al-11Mg-10Mo ternary alloy were sputtered and subjected to a heat treatment matrix of 400°C, 500°C and 600°C for 1, 2, and 8 h. Indexing the peaks in alloys that precipitated was difficult because the preferential growth of the sputtered alloys changed peak intensity ratios and some peaks were not present in the XRD spectrum. In addition, by intermixing the Al and Mo on the atomic level via sputtering, the precipitation process was approached from a different starting point than the previous investigations of the Al-Mo system by powder metallurgy, melting, or diffusion couples. Therefore, phases that were expected from the literature often were not detected.

Figure 1 shows the XRD patterns for the Al-11Mo alloy after heat treatment at 400°C for 1, 2, and 8 h. The as-deposited Al-11Mo exhibited well defined peaks that were indexed to Al shifted to slightly higher angles. Although the ratio of peak heights was not consistent with the reported values for polycrystalline Al, indicating the alloy had grown along preferential orientation, this was the only Al-Mo alloy fabricated during this work that was crystalline. A lattice parameter of 0.4004 nm was calculated from the Al (111) peak, which was shifted from the normal angle of 38.4° to 38.94°. This peak shift was consistent with adding Mo in solid solution in the Al.

After heat treating the Al-11Mo alloy at 400°C for 1, 2, and 8 h, several new peaks formed and the Al peaks disappeared. The predominant phase that formed was $Al_{12}Mo$ but the intensity ratio did not match the reported values, indicating the precipitate phase was preferentially oriented. The majority of the remaining peaks were indexed to Al_5Mo. One peak at 18.85° could not be indexed to any of the Al-Mo intermetallic compounds, the Al or Mo metallic constituents, or possible silicides. Similar XRD patterns were observed for the Al-11Mo alloy heat treated at 500°C for 1, 2, and 8 h.

As-deposited Al-18Mo exhibited broad amorphous peaks at 21° and 41° [Ref 20-22] and there was no apparent change after heat treating between 1 and 8 h at 400 °C (Fig 2). However, after heat treating at 500°C for just 1 h, the amorphous peaks disappeared and several new, well-defined peaks formed. After either 1, 2, of 8 h at 500 °C, the broad

21.5° peak split into three peaks at 20.2°, 21.9°, and 24.9° These peaks migrated to slightly higher angles as the heat treatment time increased None of the peaks could be indexed to Al and it appeared that $Al_{12}Mo$, Al_5Mo, and $Mo(Si,Al)_2$ were the dominate phases

As-deposited Al-23Mo also exhibited the two broad amorphous peaks at 21.5° and 41.2° No new peaks formed during heat treating at 400°C for 1 and 2 h However, after heat treating at 400°C for 8 h, the 21.5° peak began to separate into two broad peaks centered at 21° and 26° In addition, a shoulder began to form on the 41.2° peak After heat treating at 500°C for 8 h, the 21.5° peak separated into four peaks, a well defined peak at 23°, and three broad peaks at 17.5° 21.2°, and 26° (Fig 3). Similarly, several shoulder peaks began to form on the high angle side of 41.2° peak, with the main 41.2° peak becoming much sharper at its apex Sharpening and formation of the small peaks is likely due to the formation of nano-crystalline Al and intermetallic phases [Ref 23] After heat treating up to 600°C for 2 h, the two main amorphous peaks were found to remain fairly broad although the angle shifted slightly Precipitation and full loss of the amorphous peaks occurred only after heat treating at 600°C for 8 h

Observed peaks after heat treating at 600°C for 8 h for the Al-23Mo were indexed to Al and $Mo(Si,Al)_2$ A lattice parameter for the shifted Al of 0.403 nm was calculated. From this lattice parameter, the concentration of Mo in Al was estimated to be approximately 7 at. % This lower-than-expected molybdenum concentration is a result of Molybdenum being consumed by the Si substrate to form $Mo(Si,Al)_2$ during the heat treatment. However, a significant amount of Mo still remains in solid solution to protect the alloy from pitting.

As-sputtered ternary Al-11Mg-10Mo alloys also exhibited amorphous XRD peaks However, the ternary alloys precipitated and formed oxides and spinels with the sapphire wafer during heat treating

3.4 Polarization Testing

As-Deposited Alloys -- Table 1 and Figure 4 summarize the results of the anodic polarization experiments for the binary Al-Mo and ternary Al-Mg-Mo nonequilibrium alloys E_{oc} for all of these alloys was measured to be between -600 to -450 mV_{SCE} with the majority of the measured E_{oc} values in the range from -520 mV_{SCE} to -580 mV_{SCE}. For the Al-Mo alloys tested, i.e., with Mo concentrations greater than 5 at % Mo, no trend in E_{oc} as a function of solute concentration was apparent This agrees with earlier work [Ref 10-13] where it was found that the E_{oc} increased from 1 to 5 at % Mo, but as the concentration rose above 6 at % Mo, the E_{oc} saturated and no longer increased with increasing Mo concentration Figure 5 shows that the E_b monotomically increased with Mo concentration in the alloy The data show that initially an increase in solute concentration rapidly increased E_b, but the effect became less pronounced for the composition range between 11 and 25 at % Mo

Passive current densities for the as-deposited Al-Mo alloys were in the range of approximately 0.1 to 10.0 $\mu A/cm^2$, but no correlation between solute concentration and i_{pass} was evident Variations in i_{pass} were attributed to defects, i.e., scratches, pinholes, etc in the alloy film

Additional polarization experiments were conducted on the Al-18 Mo in either aerated or quiescent NaCl solutions, with concentration of NaCl at either 0 1M or 0 55M (3 15 wt. %), pH 8. Figure 6 shows that the polarization response was not significantly altered by increasing the chloride concentration.

SEM examination and EDS analysis of a newly formed pit on the as-deposited Al-18Mo specimen immediately after polarization to the breakdown potential showed the Mo concentration had risen from 18 at. % to 25 at. % in the pit (Fig 7), and breakdown appeared to be related to the preferential dissolution of Al from the alloy which is consistent with x-ray photoelectron spectroscopy work conducted during earlier studies [Ref 12]

SEM examination of the Al-11Mg-10Mo alloy showed that the pits formed in clusters and EDS analysis showed that no Mg remained in the alloy within the pit region In addition, directly adjacent to pits in the Al-Mg-Mo alloys, the Mg concentration had dropped to 1 9 at. %. Depletion of Mg in both the pit and surrounding alloy indicates Mg was preferentially dissolved during propagation of the pit In addition, the Mo concentration had dropped from 10 to 2.5 at. % within the pit Depletion of Mo was unexpected since the Mo concentration remained constant in the binary alloys during pit propagation

Heat Treated Alloys -- The polarization response of as-deposited and heat treated Al-11Mo alloys is shown in Figure 8. Although the E_b for the heat treated Al-11Mo alloys decreased from ~420 mV_{SCE} to 50 mV_{SCE}, the E_{oc} remained constant at approximately -550 mV_{SCE} In addition, the i_{pass} decreased from 1$\mu A/cm^2$ for the as-deposited alloy to 0 1 $\mu A/cm^2$ after heat treatment.

Both E_{oc} and E_b for the Al-18Mo alloys were not affected by heat treatment of up to 500°C for 2 h (Fig 9). The open circuit potential for all the alloys was about -550 mV_{SCE}. Similar to Al-11Mo i_{pass} for the heat treated Al-18Mo specimens was less than that for the as-sputtered alloy, with the exception of specimen heat treated at 400°C for 1 h SEM of the heat treated alloys after polarization showed crack pattern morphology in the alloy surrounding pits (Fig 10) The crack morphology was not found after heat treating and must have formed during polarization testing. These cracks were attributed to failure in the alloy caused by residual tensile stresses built up during deposition (nucleation and thermal expansion stresses) and cooling from heat treatment temperatures (thermal expansion stresses), compounded by additional stresses generated during the preferential dissolution of Al during polarization.

The Al-11Mg-10Mo alloy also exhibited an E_{oc} of approximately -580 mV_{SCE} in the as-deposited condition similar to the Al-Mo alloys (Fig 11) The E_{oc} value was maintained after heat treating at 400°C for 1 h However, heat treating the alloys at longer times and higher temperatures made the E_{oc} more active with a value of approximately -800 mV_{SCE} and no passivity was observed

3.5 Galvanic Corrosion Behavior

Galvanic diagrams (Fig 12) based on equal metal/graphite areas showed that corrosion for pure Al coupled to Gr was cathodically controlled where the pitting region of the anodic Al curve intersects the current limited region of the P75 cathodic curve at a

high current density value of 12.5 μA. As was predicted and confirmed during early Gr/Al corrosion experiments, high corrosion rates of sputtered Al coupled to P75 fibers were observed [Ref 1-4]. In addition, as the ratio of Gr-to-Al is increased the cathodic curve is shifted to higher current densities, which further increases the corrosion rate of the Al matrix.

For the Al-Mo alloys, galvanic corrosion was anodically controlled, as shown in Figure 13, by the cathodic curve intersecting the Al-Mo alloy anodic curve in the passive region. Changing the Gr-to-Al ratio and subsequently shifting the cathodic curve to higher current density values (or anodic curve to lower current density) values does not change the corrosion rate because the cathodic curve still intersects the passive region of the anodic curve (i.e., the reaction remains anodically controlled).

The galvanic diagrams also show that the galvanic corrosion reaction remains anodically controlled on the heat treated alloys that exhibited a passive region (Figs. 14-15). Intermetallic precipitates were observed in the Al-11Mo alloy after heat treatment at all times and temperatures, but because E_b for the alloy remained more noble than E_{oc} for the cathodic reaction, the galvanic current values were still anodically controlled. Only after heat treating the Al-11Mo to 500°C for 8 h was control for the galvanic reaction changed from anodic (Al passivation) to cathodic (hydrogen evolution on graphite).

Galvanic corrosion of the heat treated Al-18Mo alloys, as shown in the galvanic diagrams in Figure 15, was also controlled by the anodic Al dissolution reaction. Specimens heat treated above 500°C exhibited intermetallic precipitates but the reaction remained anodically controlled.

Galvanic currents were measured for graphite coupled to either as-deposited or heat treated Al-Mo alloys and these results are compared to commercially pure Al in Figure 16. In general, the galvanic current measured for the Al-Mo alloy was an order of magnitude lower than pure Al, although heat treating the alloy did increase the galvanic current when coupled to graphite. The average galvanic current value for as-deposited Al-18Mo was 0.04 μA (0.04 μA/cm^2) as seen in Figure 16 where-as the measured galvanic current for pure Al reached values of up to 30 μA (30 μA/cm^2). This result suggests that the protection imparted by the addition of molybdenum is reduced through heat treating the alloy. Earlier work indicated that the formation of second phase precipitates in the alloy may have contributed to the decreased resistance to pitting [Ref 11].

4.0 DISCUSSION

XRD examination indicated most of the Al-Mo alloys were amorphous even though the substrate was allowed to heat to approximately 100°C during the sputtering process. The broad peak at 21° can be attributed to short range order associated with the Al_xMo_y intermetallic compounds which have high intensity peaks at these low angles. Similarly, the broad peak at 41° was indexed to amorphous Al and is indicative of what has been found for other sputtered and rapidly solidified Al alloys [Ref 20-22]. XRD indicated Mo had not precipitated to form Al_xMo_y intermetallic compounds and thus was available for incorporation into the passive film according to the process described during previous work [Ref 1-4]. Alloys that did not form precipitates during heat treatment exhibited E_{oc} and E_b values very similar to the as-deposited alloys, whereas E_{oc} remained similar to

the as-deposited alloys but E_b was more electrochemically active for heat treatments which produced precipitates. For the Al-18Mo alloy, a noble breakdown potential of approximately 400 mV_{SCE} was observed even though secondary phases had precipitated indicating that the Mo concentration in solid solution was sufficient to form a protective passive film.

Galvanic corrosion for all of the as-deposited Al-Mo alloys was controlled by the anodic reaction. Because E_b for the anodic reaction is more noble than the E_{oc} for the cathodic reaction, Al-Mo alloys coupled to graphite fibers are expected to be stable regardless of the area ratios, even for the alloys in which secondary phases had precipitated during heat treatment (Fig 14). Decreasing the anode area (or conversely increasing the cathode area) results in lateral displacement of the polarization curves, therefore the reaction remains anodically controlled (Fig 17).

Hihara measured the cathodic reaction of P100 graphite fibers in an aerated 3.15 wt % NaCl solution [Ref 4]. Superimposing his results onto our galvanic diagrams showed the cathodic reaction on the P100 graphite fibers in a higher chloride concentration solution was very similar to the P75 graphite fiber cathodic reaction in 0.1M NaCl, pH 8 (Fig 19). The cathodic open circuit potential for both P75 and P100 graphite fibers was approximately 0 mV_{SCE}. Figure 19 shows that the Al-Mo alloys would also be galvanically stable with higher modulus graphite fibers such as P100 Gr fibers. In addition, the Al-Mo would be electrochemically stable with other reinforcements such as SiC and with fiber coatings such as TiB_2. This result is significant because it is the first time that corrosion of these types of composites has been shown to be under anodic control in chloride environments.

To confirm the predictions made using the galvanic diagrams, long term galvanic current tests were conducted on sputtered Al, Al-11Mo, Al-18Mo, Al-23Mo, and ternary Al-11Mg-10Mo in the as-deposited condition by coupling the alloy to P75 Gr fibers. Figure 16 showed the galvanic current measured as a function of time over a period of one week for the Al-18Mo alloy. For all the alloys, the galvanic current data shown in Figure 18 initially starts off at relatively high values between 3 and 30 μA (3 and 30 $\mu A/cm^2$), but quickly drops to a low steady state value. Galvanic current for the Al-11Mo specimen first leveled off at 2 μA (2 $\mu A/cm^2$) after the first day, but then monotonically decreased for the remainder of the test reaching a value of 0.04 μA (0.04 $\mu A/cm^2$) after six days. The Al-18Mo and Al-23Mo reached low measured galvanic currents (0.04 and 0.08 μA, respectively) almost immediately. These galvanic currents were three orders of magnitude lower than the galvanic current values (up to 30 μA) measured for pure sputtered Al. After galvanic testing the Al completely dissolved from the Si whereas the Al-Mo alloys remained intact and highly specular.

Up to this point, the key factors in evaluating the nonequilibrium aluminum molybdenum for use as the matrix alloy for graphite/aluminum composites was corrosion behavior and the ability to maintain the good corrosion resistance after heat treating to nominal composite consolidation temperatures. However, there is an additional factor in selecting the optimum matrix alloy for Gr/Al that was inferred by investigation of the Mg addition, this is density. With the addition of molybdenum to aluminum, the density increases and will begin to approach that of titanium. Titanium exhibits good corrosion resistance and is one of the few metals that is electrochemically stable when galvanically coupled to graphite. Because corrosion resistance and alloy thermal stability were found

to increase with increasing molybdenum concentration. If density were not a concern, the best alloy would be the alloy with the highest concentration of Mo

In order to evaluate the effect of molybdenum addition to aluminum, density was predicted by substituting molybdenum atoms in the face center cubic aluminum lattice structure. Although it has already been shown the material is amorphous, the atomic ratios and packing should be similar. At the very least it provides a conservative density as a function of molybdenum addition, because a face center cubic structure is close packed and hence will be a higher density than an amorphous alloy. In addition, it was assumed that the volumetric contraction of the unit cell by the incorporation of the smaller molybdenum atoms in the aluminum lattice was negligible

The density of the aluminum-molybdenum alloy can be calculated by the following relationship

$$\rho_T = \frac{w_1 + w_2}{V_T}$$

where ρ_T is the total alloy density, w is the weight, V_T is the total volume, and the subscripts 1 and 2 represent molybdenum and aluminum, respectively. This expression can be related to fundamental known quantities of atomic fraction, X, number of atoms per unit cell, n, lattice parameter, a, and density of the solute and solvent, ρ, as follows

$$\rho_T = \rho_1 X_1 \frac{n_2 a_2^3}{n_1 a_1^3} + (1 - X_1)\rho_2$$

Using the above expression density as a function of atomic fraction molybdenum showed that the alloy density approaches that of titanium at about 22 atomic percent. Density for the Al-18Mo alloy which also exhibited good corrosion behavior after heat treating to 500°C for eight hours was predicted to be approximately 4000 kg/m^3 compared to 4510 kg/m^3 for titanium. Measured densities were approximately 75% of the values predicted using the relationship above

5.0 CONCLUSIONS

Nonequilibrium aluminum-molybdenum alloys made by magnetron sputtering during this work have clearly been shown to be compatible matrix alloys for graphite/aluminum composites. The Al-Mo alloys maintain their corrosion resistance after heat treating to nominal composite processing temperatures between 400 and 500°C. In addition, the Al-Mo alloys coupled to P75 graphite fiber exhibited extremely low corrosion currents. Because the breakdown potential for the anodic reaction is significantly more noble than the open circuit potential for the cathodic reaction, the aluminum-molybdenum alloys will be electrochemically stable when coupled to graphite fibers regardless of the area ratios in a 0.1M NaCl electrolyte. Therefore, aluminum alloyed with 10 to 26 atomic percent molybdenum provides a matrix that can be processed and consolidated at high temperatures and still retain its inherent corrosion resistance with the graphite fiber in the composite. The optimum alloy composition was Al-18Mo. This alloy was the lowest density (4000 kg/m^3) material that exhibited an anodic controlled reaction when coupled

to graphite, and was stable during heat treatment to nominal composite consolidation temperatures.

Summarizing the significant results of this work:

1.) X-ray diffraction of the alloys demonstrated that aluminum with 18 to 23 atomic percent molybdenum could be heat treated up to 400°C for 8 hours without detectable precipitation or change in corrosion behavior. In addition, the Al-23Mo could be heat treated to 600°C for two hours without degrading the corrosion performance.

2.) Al-18Mo heat treated at 400°C for eight hours exhibited a corrosion potential of -556 mV_{SCE}, a breakdown potential of 335 mV_{SCE} and passive current density of 0.4 $\mu A/cm^2$ in a 0.1 M NaCl, pH 8 solution. These values are very similar to the as-sputtered Al-18Mo alloys and are a significant improvement over pure aluminum.

3.) Galvanic current densities measured for Al-18Mo and Al-23 Mo of 0.04 to 0.08 $\mu A/cm^2$ were 3 orders of magnitude lower than the 30 $\mu A/cm^2$ measured for pure Al in the 0.1 M NaCl, pH 8 solution when coupled to P75 graphite fibers.

4.) Ternary Al-Mg-Mo alloys exhibited a lower density than the Al-Mo alloys; however, the addition of Mg to Al-Mo alloys appears to be deleterious from the standpoint of improving passivity.

ACKNOWLEDGMENTS

The authors would like to gratefully thank John Sedriks for his support. This work was funded the by Office of Naval Research under contract N00014-91-J-1196. Commercial equipment is identified in the paper to specify the experimental procedure.

REFERENCES

1. L.H. Hihara, Corrosion of Aluminum-Matrix Composites, Ph.D. Dissertation, Massachusetts Institute of Technology, (1985).

2. L.H. Hihara and R.M. Latanision, "Residual Microstructural Chloride in Graphite-Aluminum Metal Matrix Composites," Material Science Engineering A, 1990, vol. 126, pp. 231-234.

3. L.H. Hihara and R.M. Latanision, "Localized Corrosion Induced in Graphite/Aluminum Metal-Matrix Composites by Residual Microstructural Chloride," Corrosion, 1991, vol. 47, pp. 335-340.

4. L.H. Hihara and R.M. Latanison, "Galvanic Corrosion of Aluminum-Matrix Composites," Corrosion, 1992, vol. 48, pp. 546-552.

5. W.C. Harrigan and R.H. Flowers, "Graphite-Metal Composites Titanium-Boron Vapor Deposit Method of Manufacture," Failure Modes in Composites IV, J.A. Cornie and F.W. Crossman, eds., The Minerals, Metals, and Materials Society, Warrendale, PA, 1977, pp. 319-335.

6. I.J. Toth, W.D. Brenthall, a[illegible] G.D. Menke, "A Survey of Aluminum Matrix Composites," Composites: State of the Art, [illegible] Weeton and E. Scala, eds., The Minerals, Metals, and Materials Society, Warrendale, PA, 19[illegible] p. 139-207.

7. J.H. Payer and P.G. Sulliv[illegible], "Corrosion Protection Methods for Graphite Fiber Reinforced Aluminum Alloys," Bicentennial of Materials, Society for the Advancement of Material and Process Engineering, Azusa, CA, 1976 vol. 8, pp. 343-352.

8. V.C. Nardone and J.R. Strife, "Advanced Gr/Mg Composite Development," United Technologies Research Center, Interim Report R89-917711-4, East Hartford, CT, July 1989.

9. R.J. Weimer, W.F. Henshaw, T.G. Casswell, B.D. Dickerson, J.P. Hickerson, and S.D. Shelton, Fabrication of Thin-Walled Seamless Tubes from Gr/Mg Precursor Tapes, Cordec Corporation, Lorton, VA, 1992.

10. W.C. Moshier, G.D. Davis, J.S. Ahearn, and H.F. Hough, "Influence of Molybdenum on the Pitting Corrosion of Aluminum Films," Journal of the Electrochemical Society, 1986, vol. 133, pp. 1063-1064.

11. W.C. Moshier, G.D. Davis, J.S. Ahearn, and H.F. Hough, "Corrosion Behavior of Aluminum-Molybdenum Alloys in Chloride Solutions," Journal of the Electrochemical Society, 1987, vol. 134, pp. 2677-2684.

12. W.C. Moshier, G.D. Davis, and G.O. Cote, "Surface Chemistry of Sputter-Deposited Al-Mo and Al-Cr Alloys Polarized in 0.1M KCl," Journal of the Electrochemical Society, 1989, vol. 136, pp. 356-362.

13. G.D. Davis, W.C. Moshier, G.G. Long, and D.R. Black, "Passive Film Structure of Supersaturated Al-Mo Alloys" Journal of the Electrochemical Society, 1991, vol. 138, pp. 31943199.

14. G.S. Frankel, M.A. Russak, C.V. Jahnes, M. Mirzamaani, and V.A. Brusic, "Pitting of Sputtered Aluminum Alloy Thin Films," Journal of the Electrochemical Society, 1989, vol. 136, pp. 1243-1244.

15. G.D. Davis, W.C. Moshier, T.L. Fritz, and G.O. Cote, "Evolution of the Chemistry of Passive Films of Sputter-Deposited, Supersaturated Al Alloys," Journal of the Electrochemical Society, 1990, vol. 137, pp. 42.

16. B.A. Shaw, L. Fritz, G.D. Davis, and W.C. Moshier, "Influence of Tungsten on the Pitting of Aluminum Films," Journal of the Electrochemical Society, 1990, vol. 137, pp. 1317.

17. B.A. Shaw, G.D. Davis, T.L. Fritz, B.J. Rees, and W.C. Moshier, "The Influence of Tungsten Alloying Additions on the Passivity of Aluminum," Journal of the Electrochemical Society, 1991, Vol. 138, pp. 3288.

18. G.D. Davis, B.A. Shaw, B.J. Rees, and M. Ferry, "Mechanisms of Passivity of NonequilibriumAl-W Alloys," Journal of the Electrochemical Society, 1993, Vol. 140, pp. 951.

19. T.R. Schrecengost, B.A. Shaw, R.G. Wendt, and W.C. Moshier, "Nonequilibrium Alloying for Improving the Corrosion REsistance of Graphite Reinforced Al Metal Matrix Composites," Accepted by Corrosion.

20. D.A. Jones, Principles and Prevention of Corrosion, 1st ed., Macmillian Publishing Co. New York, NY, 1992, pp. 167-188.

21. P. Furrer and H. Warlimont, "Crystalline and Amorphous Structures of Rapidly Solidified Al-Cr Alloys," Materials Science and Engineering, 1977, vol. 28, pp. 127-137.

22 K. Asami, H. Yoshioka, K. Hashimoto, K. Shimizu and K. Kobayashi, "Superlattice-Like Structure of Sputter-Deposited Amorphous Aluminum-Heavy Element Alloys," Journal of Non-Crystalline Solids, 1989, vol. 110, pp. 258-264.

23 Y. He, S.J. Poon, and G.J. Shiflet, "Synthesis and Properties of Metallic Glasses That Contain Aluminum," Science, 1988, vol. 241, pp. 1640-1642.

Table 1. Alloy Composition and Anodic Polarization Data in 0.1M NaCl (pH 8) for Binary Al-Mo and Ternary Al-Mg-Mo Non-Equilibrium Alloys.

Alloy Composition (at.%)	E_{oc} (mV v. SCE)	E_b (mV v. SCE)	i_p ($\mu A/cm^2$)
Al	-1093	-690	0.1
	-1224	-689	0.7
Al-4Mo	-520	100	---
	-540	100	---
	-550	155	0.63
Al-12Mo	-550§	525	6.50
Al-26Mo	-440	750	3.0
	-427	700	0.60
	-460	600	0.80
	-495	770	1.90
	-540	760	4.17
Al-19Mo	-490	320	1.26
	-545	470	1.26
Al-11Mo	-581	220	2.69
	-629	100	23.7†
	-681	0.0	46.6†
Al-18Mo	-520	461	0.89
	-601	391	3.5
	-555	456	3.63
Al-23Mo	-582	563	45.6
	-582	492	7.6
	-591	496	7.6
Al-12Mg-13Mo	-513	55	1.0
	-573	85	4.5
	-550	39	5.6
Al-11Mg-10Mo	-555	*	*
	-494	*	*
	-542	*	*

†Alloy Started To Passivate But Then Rose to Higher Current Density Before Passivating

*Did Not Passivate

§ All alloys tested at scan rate of 0.2 mV/s except those noted with § which were tested at scan rate of 0.01 mV/s

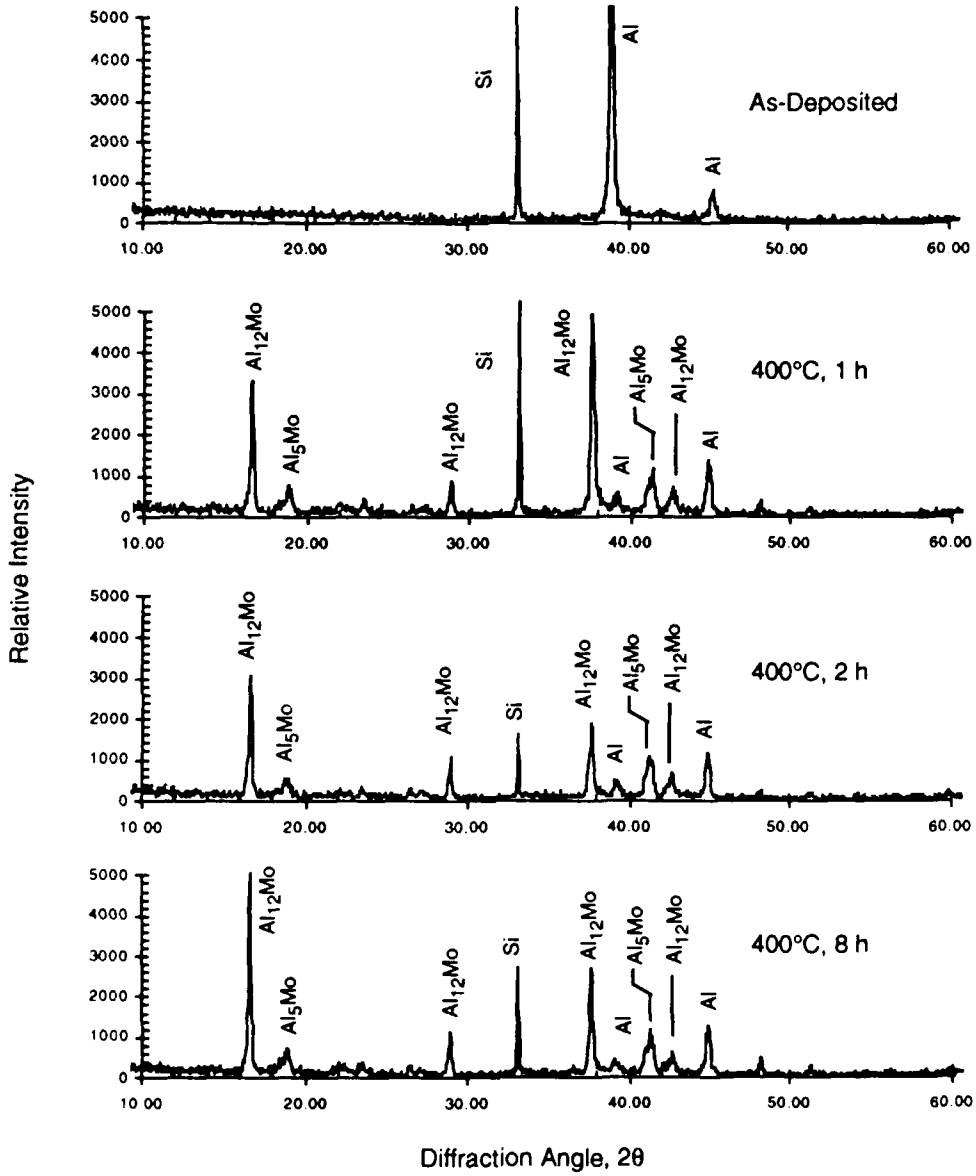

Figure 1. X-Ray Diffraction Patterns for Al-11Mo in the As-Deposited Condition and After Heat Treatment at 400°C for 1, 2, and 8 h.

earlier (Ref. 15-16) with Gr/Al composites provides a practical application to the sputtering

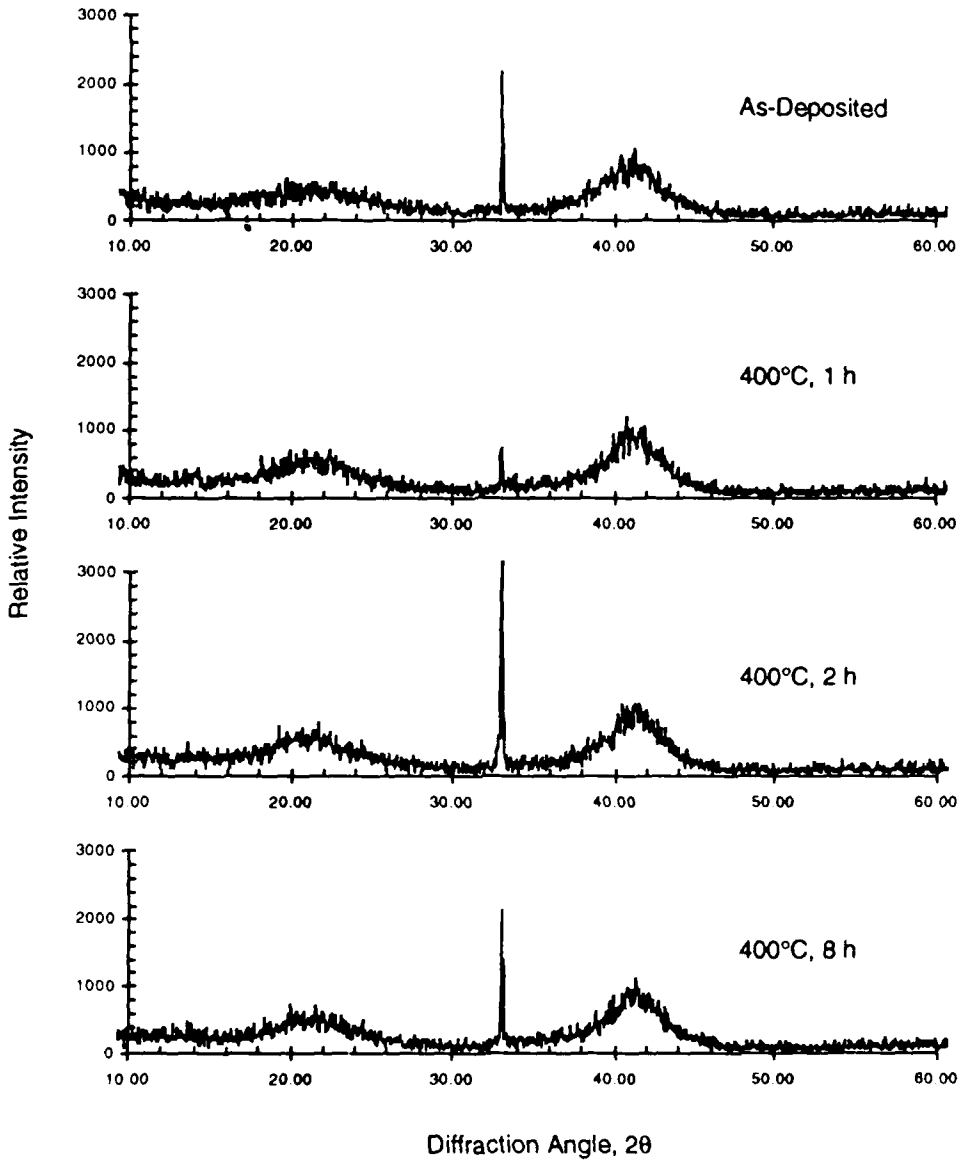

Figure 2. X-Ray Diffraction Patterns for Al-18Mo in the As-Deposited Condition and After Heat Treatment at 500°C for 1, 2, and 8 h.

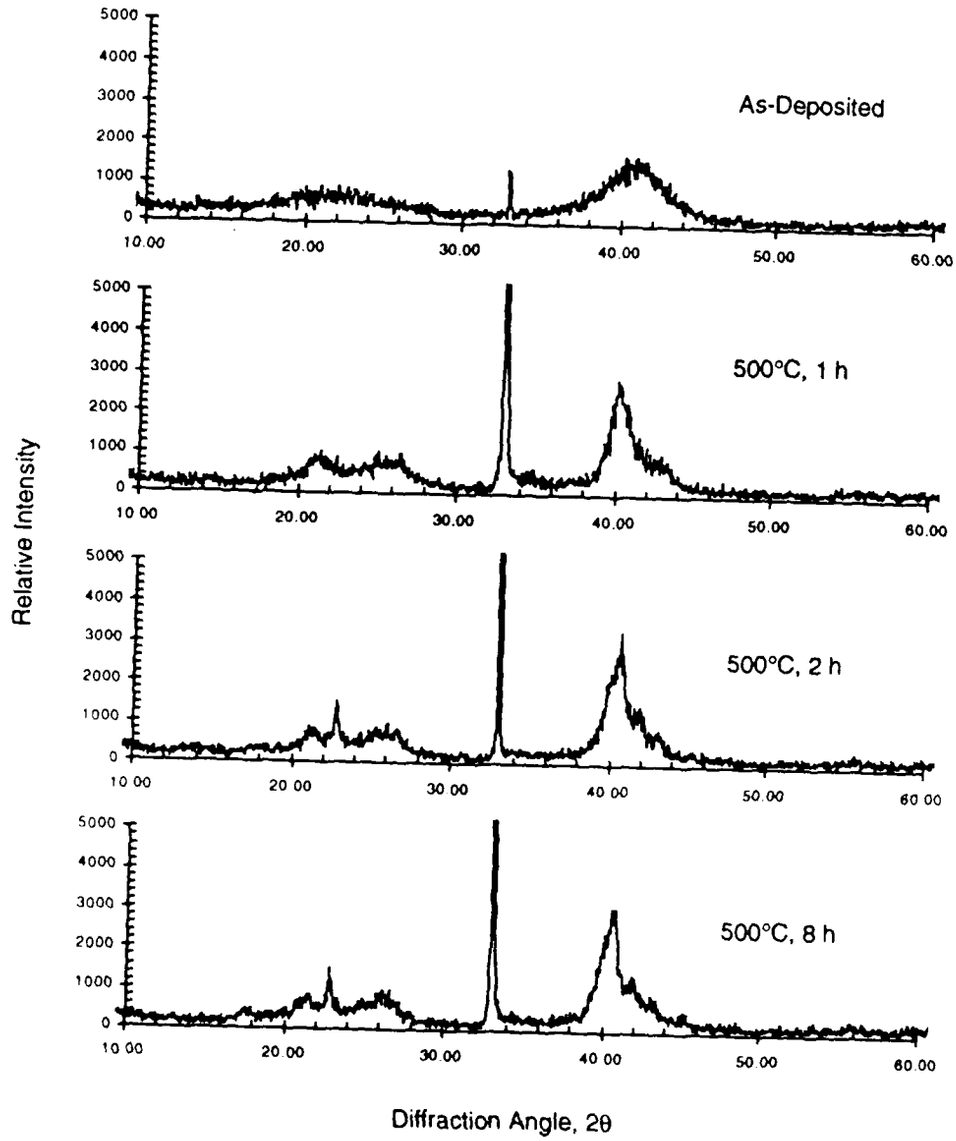

Figure 3. X-Ray Diffraction Patterns for Al-23Mo in the As-Deposited Condition and After Heat Treatment at 500°C for 1, 2, and 8 h.

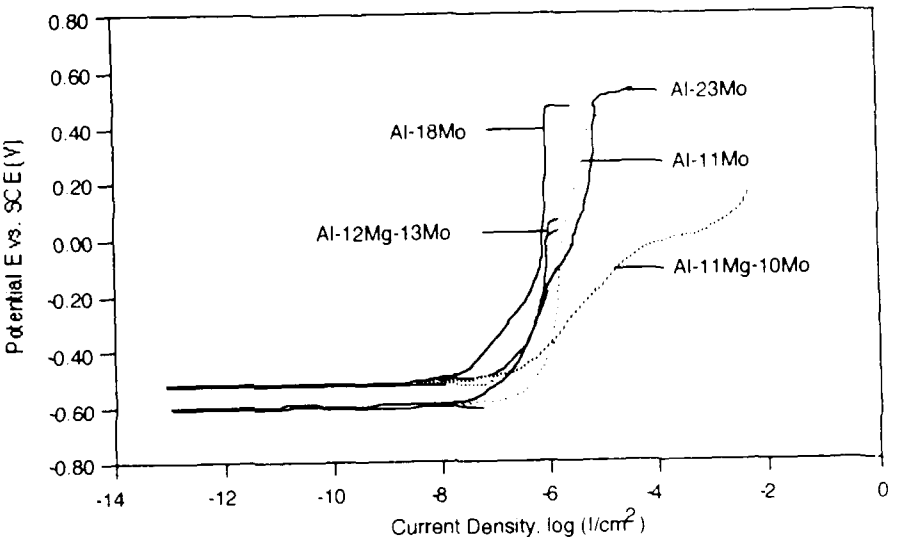

Figure 4. Anodic Polarization Response of as-deposited Al-Mo and Al-Mg-Mo Alloys, Polarized in Quiescent 0.1M NaCl, pH 8, 25°C

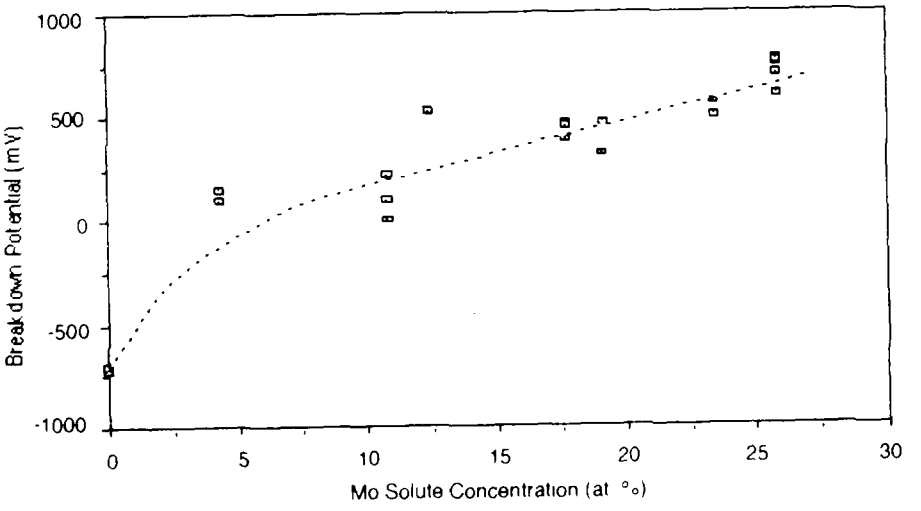

Figure 5 Breakdown Potential as a Function of Molybdenum Solute Concentration Tested in Quiescent 0 1M NaCl at pH 8, 25°C

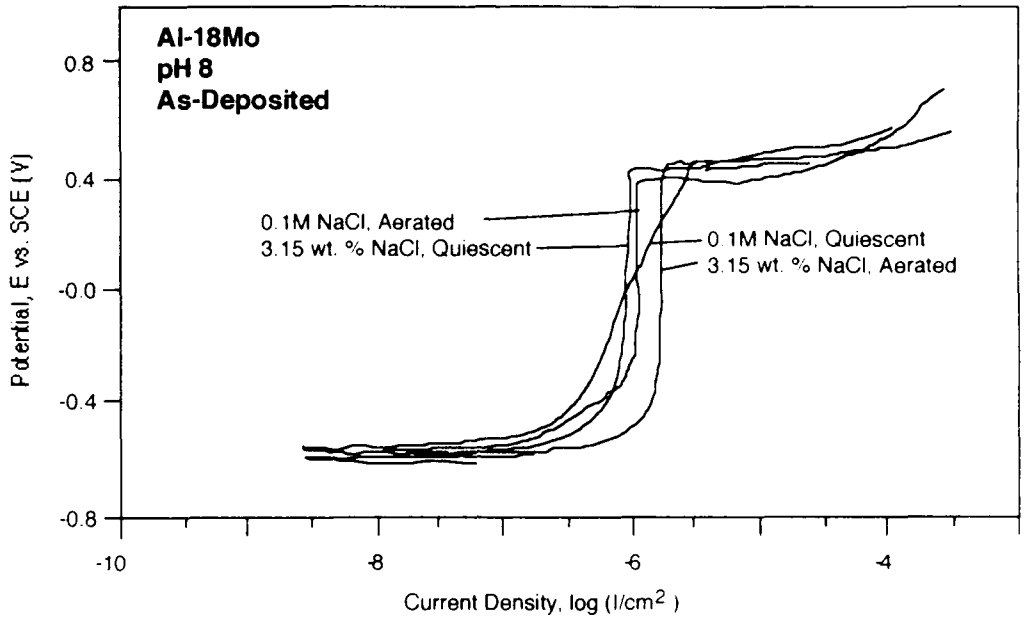

Figure 6. Anodic Polarization Response of Al-18 Mo Used for Detailed Heat Treatment Studies, Polarized in Quiescent and Aerated 0.1M and 3.15 wt. % NaCl, pH 8, 25°C

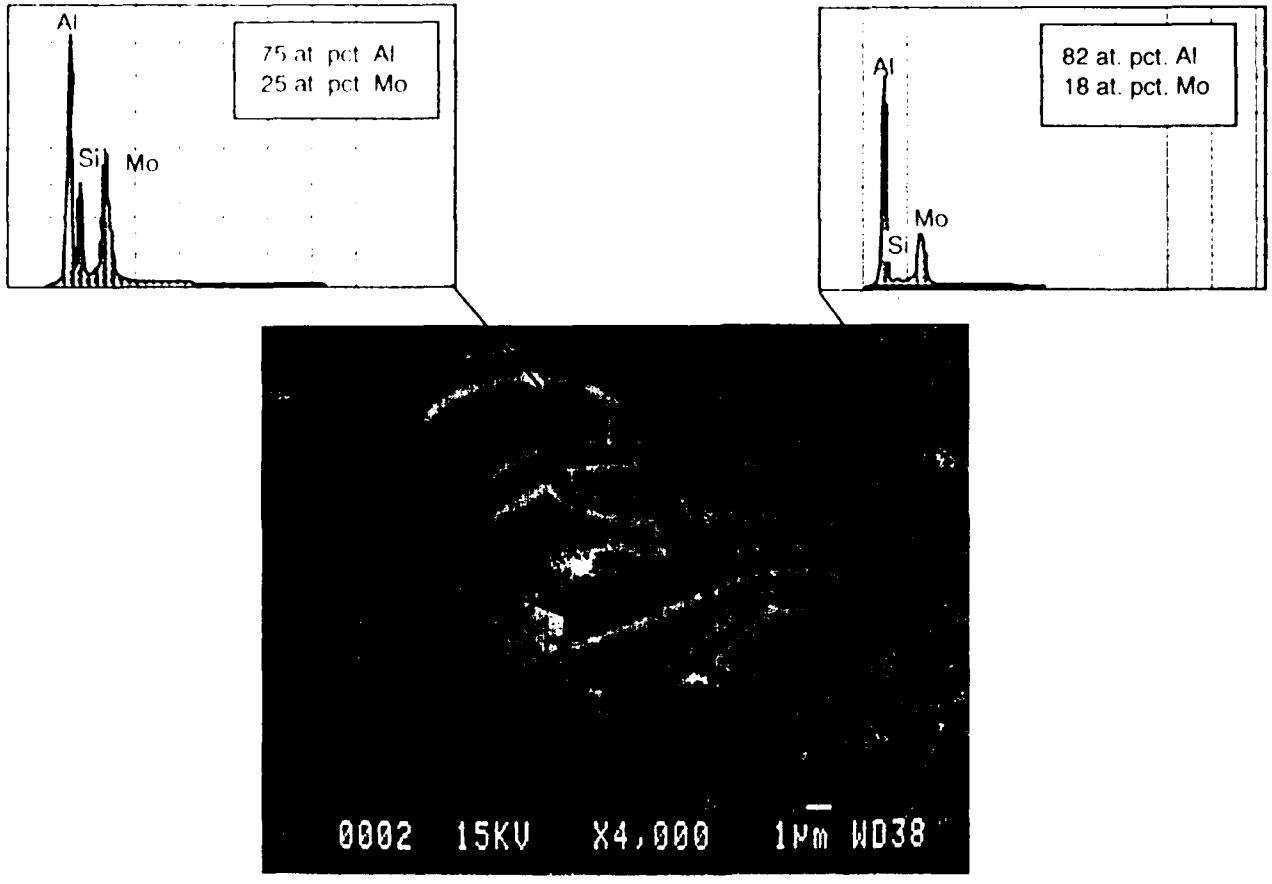

Figure 7. Newly Forming Pit In the Al-18Mo Specimen At The Breakdown Potential, EDS Analysis Indicated Aluminum Dissolution Occurring in Center Region, Quiescent 0.1M NaCl, pH 8.

E_b values very similar to the as-deposited alloys whereas E_{0s} remained similar to

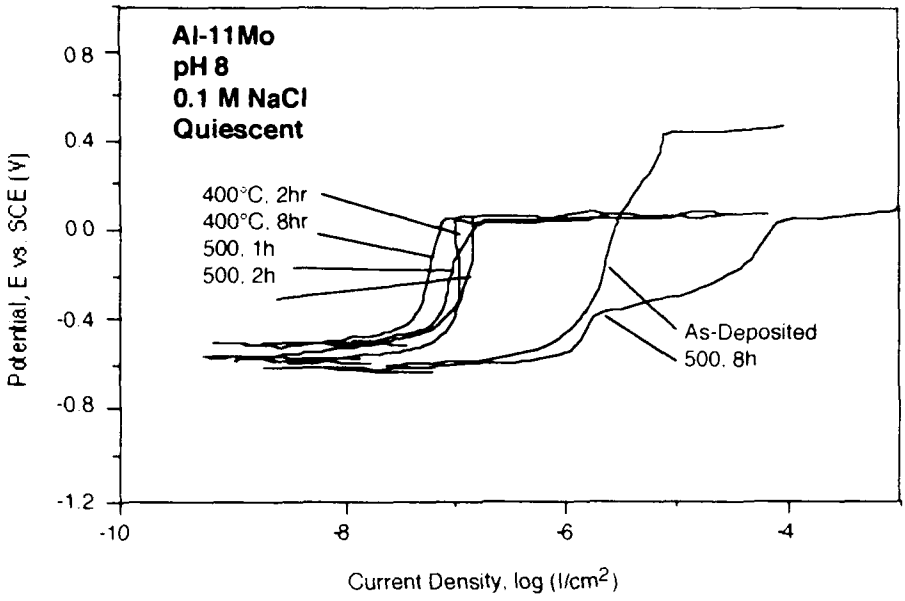

Figure 8. Anodic Polarization Response of Al-11Mo Alloy Before and After Heat Treatment at 400 and 500°C for 1, 2, and 8 h, Polarized in Quiescent 0.1 M NaCl, pH 8, 25°C.

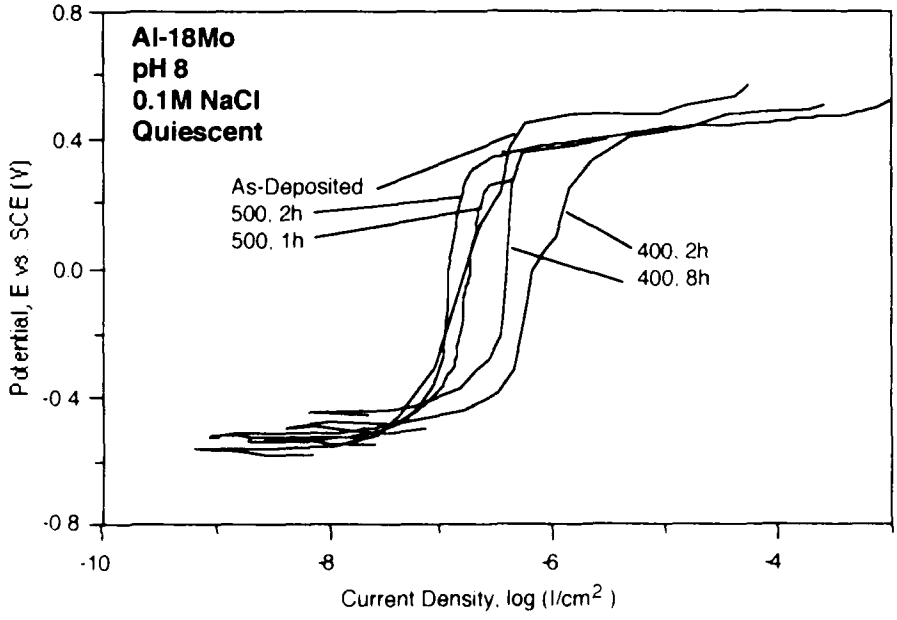

Figure 9 Anodic Polarization Response of Al-18Mo Alloy Before and After Heat Treatment at 400 and 500°C for 1, 2, and 8 h, Polarized in Quiescent 0 1 M NaCl, pH 8, 25°C

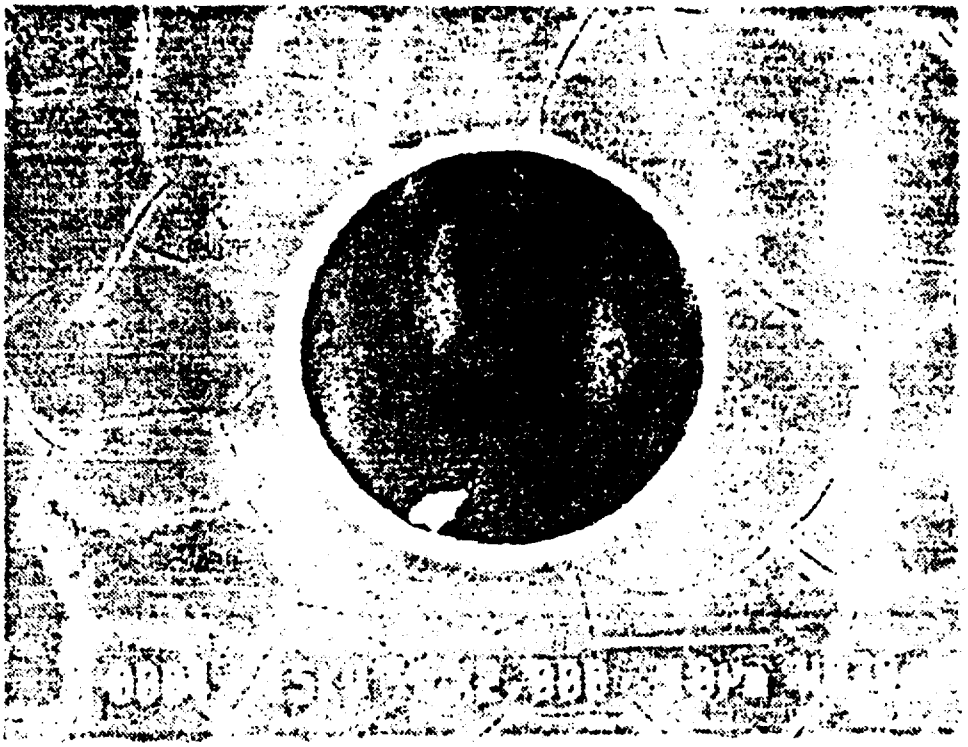

Figure 10. Circular Pit and in Al-18Mo Heat Treated At 400°C for 8 h Surrounded by Alloy Containing Mud-Crack Pattern, Tested in Quiescent 0.1M NaCl, pH 8.

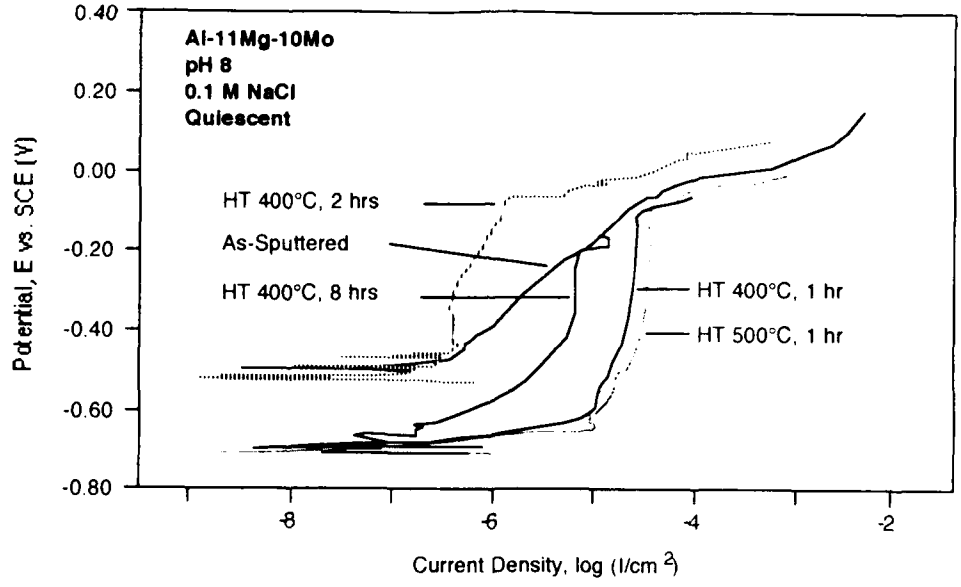

Figure 11. Anodic Polarization Response of Al-11Mg-10Mo Before and After Heat Treatment at 400°C for 1, 2 and 8 hrs and 500°C for 1 hr, Polarized in Quiescent 0.1M NaCl, pH 8, 25°C.

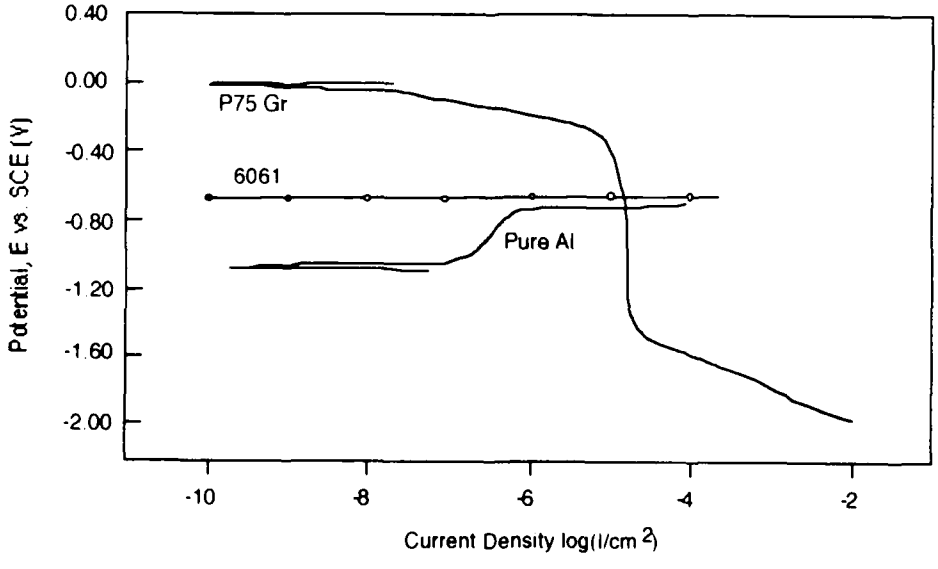

Figure 12. Galvanic Diagram for Equal Areas of Pure Aluminum and 6061 Aluminum Alloy With P75 Graphite Fibers, Tested in Quiescent 0.1M NaCl, pH 8, 25°C. (6061 Al Potentiostatic Data From Ref 4).

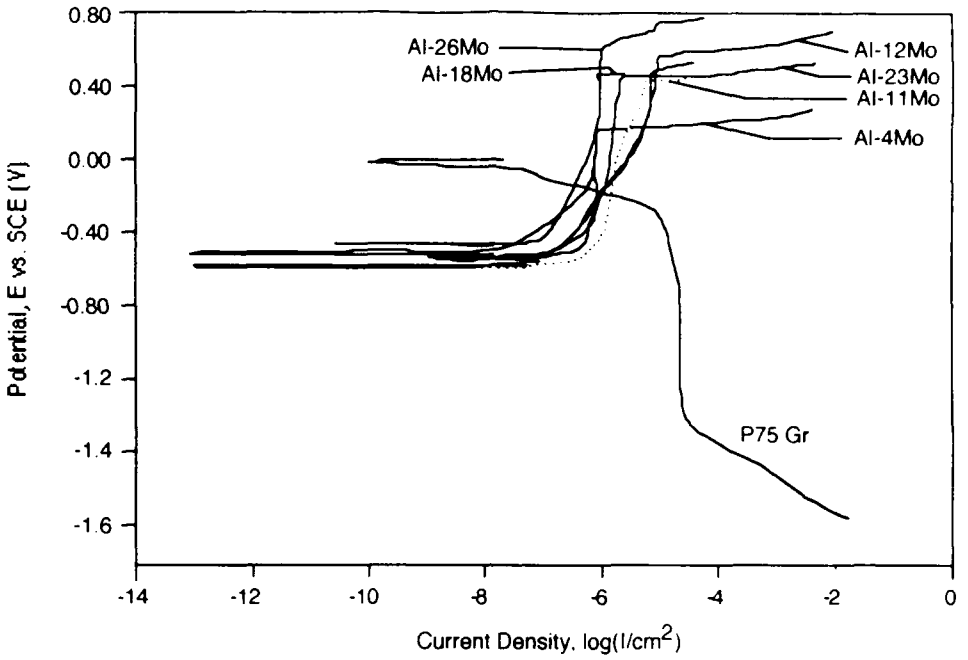

Figure 13. Galvanic Diagram for Equal Areas of Various As-Deposited Al-Mo Alloys With P75 Graphite Fibers, Tested in Quiescent, 0.1M NaCl, pH 8, 25°C.

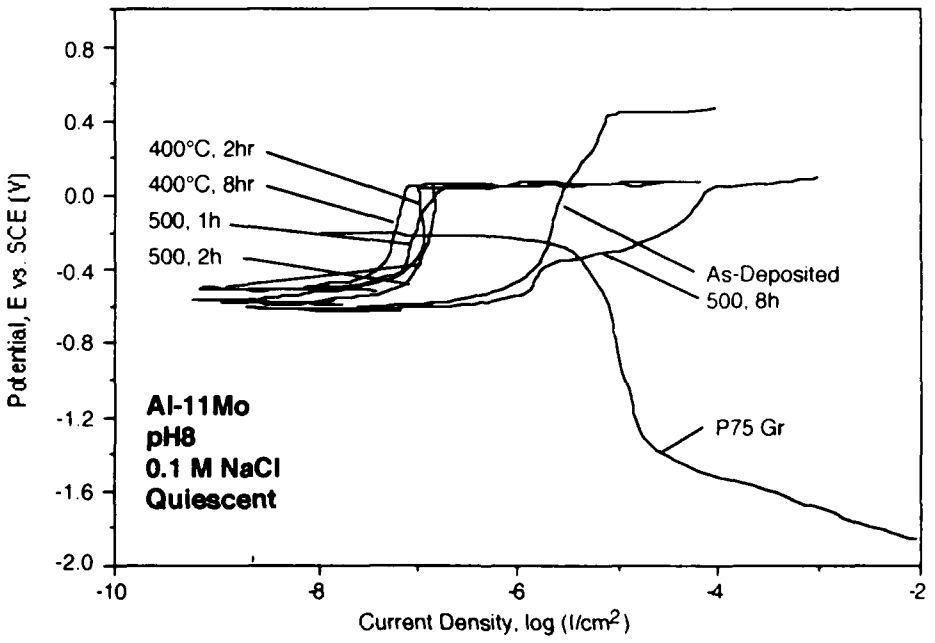

Figure 14. Galvanic Diagram for Equal Areas Al-11Mo Alloy Before and After Heat Treatment at 400 and 500°C for 1, 2, and 8 h With P75 Gr Fibers, Tested in Quiescent 0.1 M NaCl, pH 8, 25°C.

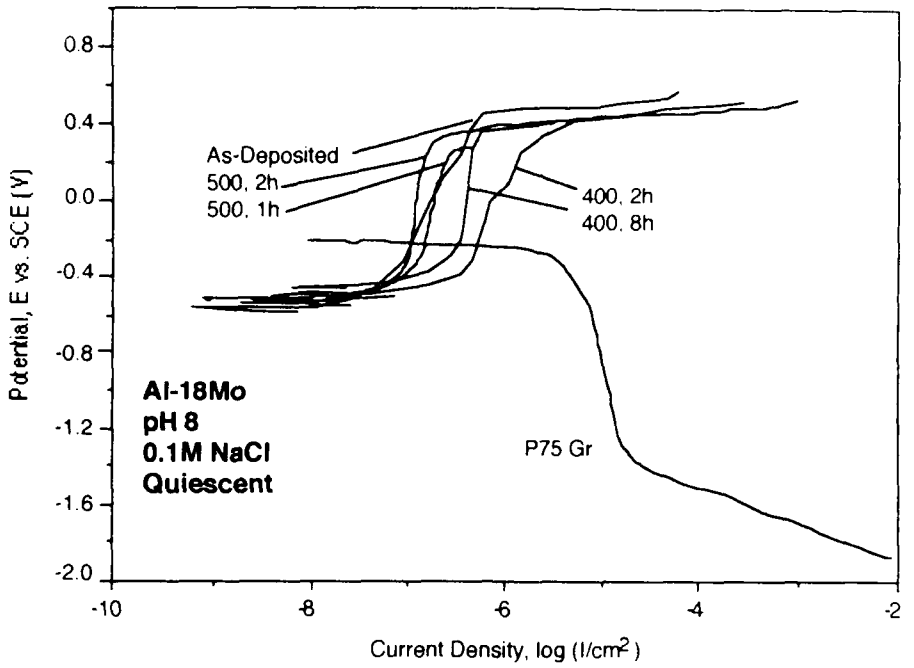

Figure 15. Galvanic Diagram for Equal Areas Al-18Mo Alloy Before and After Heat Treatment at 400 and 500°C for 1, 2, and 8 h With P75 Gr Fibers, Tested in Quiescent 0.1 M NaCl, pH 8, 25°C.

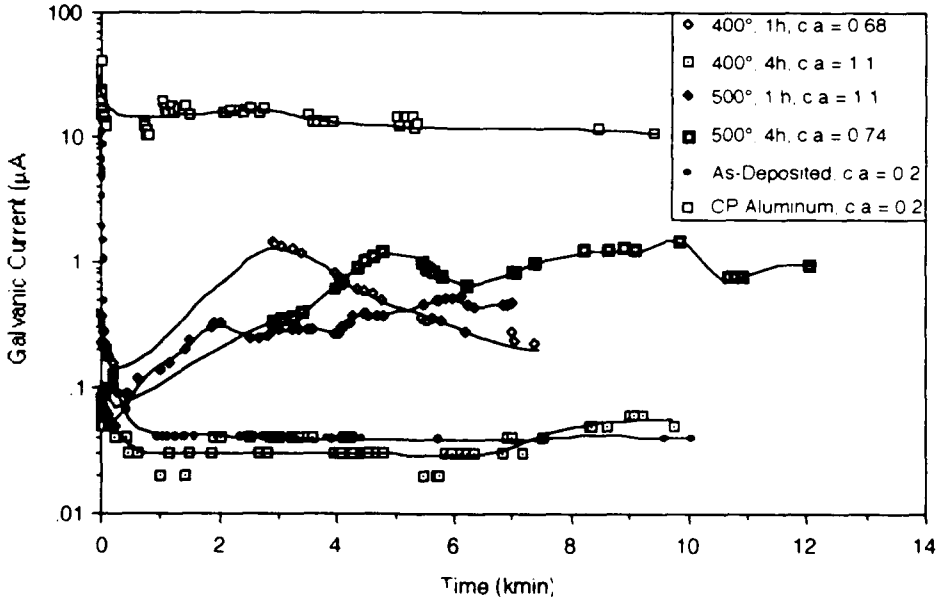

Figure 16. Galvanic Current for Commercially Pure Aluminum and Al-18Mo Alloys (As-Deposited and Heat Treated) Coupled to P75 Graphite Fibers in Quiescent 0.1M NaCl, pH 8, 25°C.

After Heat Treatment at 500°C for 1, 2, and 8 h.

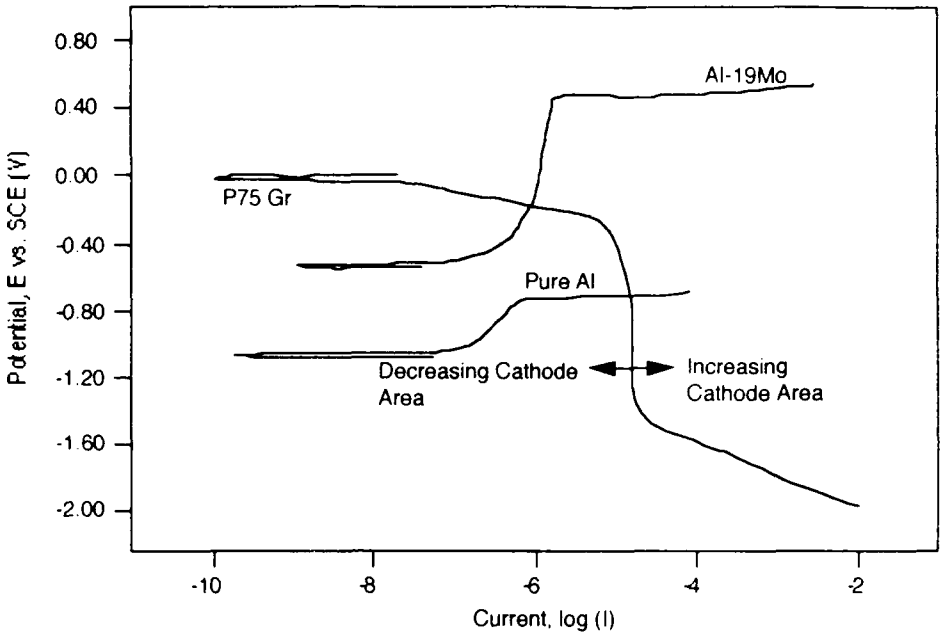

Figure 17. Affect of Changing Anode/Cathode Ratio from Equal Areas for the Al-19Mo/P75 Galvanic Couple, Tested in Quiescent 0.1M NaCl, pH 8, 25°C

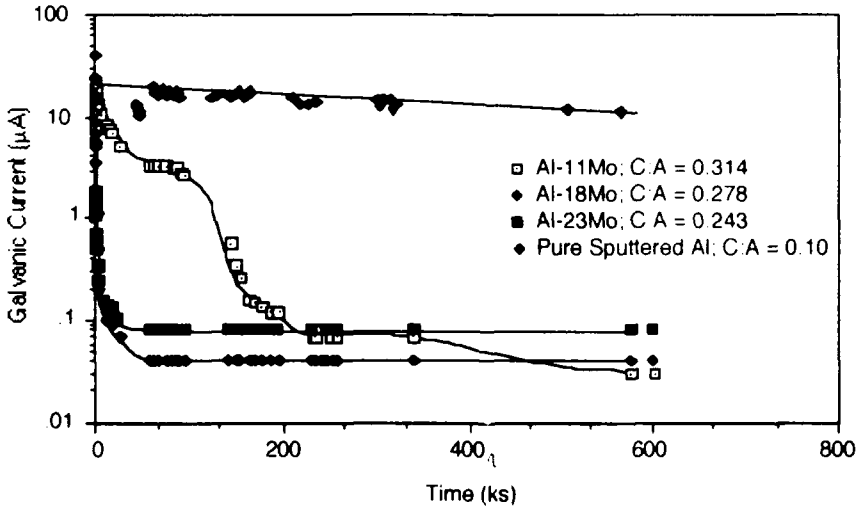

Figure 18. Galvanic Current for Pure Sputtered Al, Al-11Mo, Al-18Mo, and Al-23Mo Coupled to P75 Graphite Fibers in Quiescent 0.1 M NaCl, pH 8, 25 °C

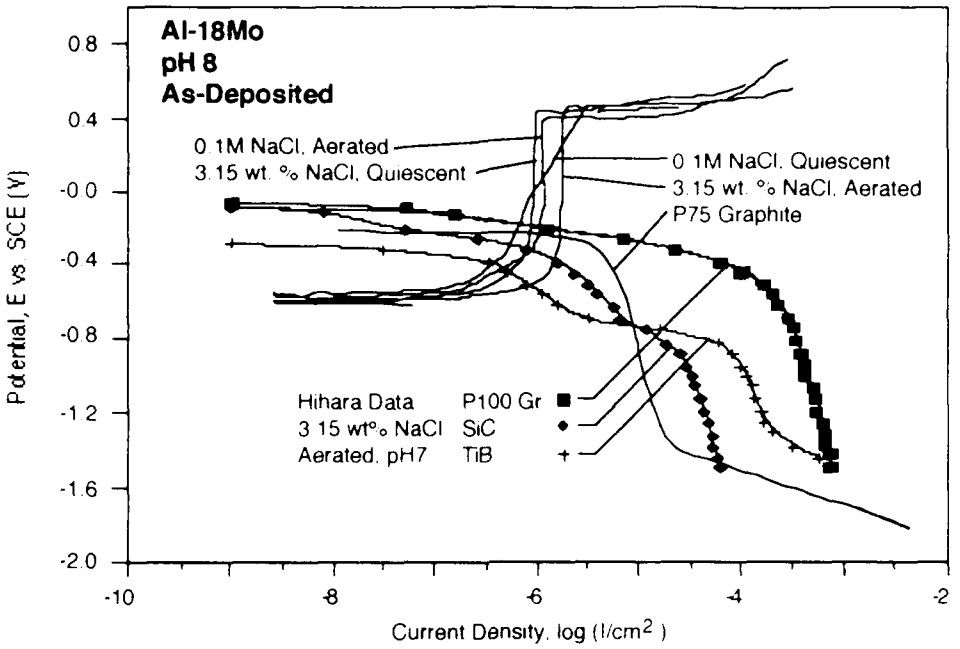

Figure 19. Anodic Polarization Response of Al-18Mo Tested in Quiescent 0.1M and 3.15 wt. % NaCl, pH 8, 25°C Superimposed with P75 Cathodic Curve and P100, SiC and TiB_2 Cathodic Data from Hihara and Latanision [Ref 4]